Earlier collapse of Anthropocene ecosystems driven by multiple faster and noisier drivers

Willcock, Simon; Cooper, Gregory; Addy, John; Dearing, John

Nature Sustainability

DOI:
https://doi.org/10.1038/s41893-023-01157-x

Published: 22/06/2023

Peer reviewed version

Contents:

SI-1: Supplementary Introduction

One perspective on the global 'tipping point' problem takes a bottom-up approach arguing that human transformation and fragmentation of the Earth surface, caused by global warming but also through land use activities, are causing many localised tipping points to be crossed[1,2]. As local thresholds are crossed, abrupt changes are seen in diverse environments (e.g. terrestrial biodiversity, fish yields, ocean oxic zones, lake water quality, water supplies[3]) with threats to the future sustainability and resilience of Earth's sub-systems[4]. Another perspective uses a top-down tipping point framework and argues that different regional 'global climate' tipping elements may change rapidly as global mean temperatures increase and thresholds are crossed[5].

Some studies draw these perspectives together; for example, Rocha *et al.*[6] explored the interactions between climate tipping elements and ecosystems in an empirical database of 30 observed and modelled regime shifts. They identified shared drivers, one-way and two-way domino cascades and two-way cascades [cf.[7]] where there are hidden feedbacks. Forty five percent of the tipping points showed evidence for structural interdependence meaning that the abrupt change observed in one system will trigger a shift in another system. Shared drivers are most common across similar land uses[6]. Potential domino effects were only found in time, not space, and related to tipping points in systems with slow temporal dynamics, such as monsoon weakening, thermohaline collapse and GIS collapse[6]. Lade *et al.*[8] extended the interrogation of existing datasets to produce a dynamic assessment of linkages. They reviewed previously studied interactions to identify a dense network of interactions between the planetary boundaries and used control theory to produce a linear equilibrium model to assess feedbacks. Only 6 out of 35 interactions identified include balancing (i.e., negative) feedbacks[8]. Their analysis indicates that the majority of the resulting cascade feedback mechanisms are reinforcing and predominantly amplifying human impacts on the Earth system, thereby shrinking the 'safe operating space' for future impacts.

SI-2: Supplementary Results

Single driver

We show that in three of the models (Easter Island, TRIFFID and Lake phosphorus), changes in primary driver strengths produce comparatively larger reductions in the absolute time before the abrupt threshold-dependent change (ATDC) is reached at low driver levels (i.e., when the primary driver is relatively weak), when compared to the same change at higher values of the primary driver, although the percentage value by which the ATDC is brought forward is relatively consistent (Figure 2). In other words, the absolute advance in the ATDC may be reduced as driver strength increases, but the percentage shift in the time point is likely similar. For example, increasing the normalised baseline driver strength from 0.3 to 0.5 decreases the median time until system collapse by 3 years (9.4%), 341 years (28.9%), 92 years (38.7%) and 245 unitless timesteps (29.0%), for Lake Chilika, Easter Island, TRIFFID, and Lake phosphorus respectively (Figure 2). In turn, increasing the normalised driver strength from 0.5 to 0.7 decreases the median time until system collapse by 4 years (13.8%), 175 years (20.9%), 40 years (27.4%), and 166 unitless timesteps (27.6%) across the four models respectively.

Multiple Drivers

Increasing the strength of multiple (i.e., secondary and tertiary) drivers further reduces the breakpoint date (Figure 2). As with a single driver, this effect is more noticeable on unit time at low driver levels, but the percentage effect is relatively consistent. For example, at a normalised driver strength of 0.3, the Easter Island model shows that the addition of two extra drivers brings the median ATDC forward from timestep 1179 to timestep 563 (reduction: 616 years [52.2%]), but the same extra drivers added to the main driver at 0.5 normalised levels only advances the date of collapse from timestep 838 to timestep 470 (reduction: 368 years [43.9%]). These results are consistent with the TRIFFID and Lake phosphorus models (TRIFFID: 76 years [31.9%] and 18 years [17.0%] reduction for one additional driver; Lake phosphorus: 187 timesteps [22.0%] and 58 timesteps [14.0%] reduction for two additional drivers, for 0.3 and 0.7 normalised primary slow driver levels respectively; Figure 2). By contrast, the addition of two extra drivers only brings forward the median ATDC in the Lake Chilika model by 1 years [2.3%] and 2 years [8%], for 0.3 and 0.7 normalised primary slow driver levels respectively – reflecting the dominance of the primary driver (i.e., the growth of the fisher population) on fishery dynamics. Variation around these median responses (Figure 2) is determined by the relative strength of the additional drivers, with the addition of a weak driver bringing forward the start of system collapse substantially less than the addition of a strong secondary driver (Figure S2-1).

Noise

Consistent across all models, the addition of low noise (defined as normalised σ values ≤ 0.333) at a normalised baseline driver strength of 0.3 has a limited impact upon the breakpoint date, ranging between advancing the date by 4.5 timesteps (0.5%) in the Lake phosphorus model to advancing the breakpoint date by 27 years (2.2%) in the Easter Island model (respective change in the Chilika model: 0 years [0%]; respective change in the TRIFFID model: 3 years [1.2%]).

However, the addition of high noise (normalised σ values > 0.666) highlights that increasing the variability of the primary slow driver (in isolation) across all four models can bring forward the date of system collapse (Figure 3). For example, at a normalised primary driver strength of 0.3 in the Easter Island model (Figure 3B), the addition of high noise brings the median ATDC forward from timestep 1179 to timestep 848 (28.1% reduction); the same levels of noise at a 0.7 normalised baseline driver strength advance the date of collapse from 663 to 290 (56.3% reduction). In turn, the equivalent advances in the breakpoints of the other three models under high noise are 11 (34.4%) and 6 (24.0%) years for Lake Chilika, 47 (19.7%) and 18 (16.5%) years for TRIFFID, and 104 (12.3%) and 61 (14.5%) timesteps for Lake phosphorus, for 0.3 and 0.7 normalised baseline driver strengths respectively. Combined, addition of low, mid and high noise levels resulted in 2.5%, 6.6%, 2.0% and 2.6% of

modelled ATDCs occurring at primary driver strengths below the minimum threshold required to result in an ATDC when acting in isolation for Lake Chilika, Easter Island, TRIFFID and Lake phosphorus respectively (Table S2-2). These results are consistent regardless of whether the noise is coupled to the magnitude of the primary slow driver or not (Figure S2-2; Table S2-3).

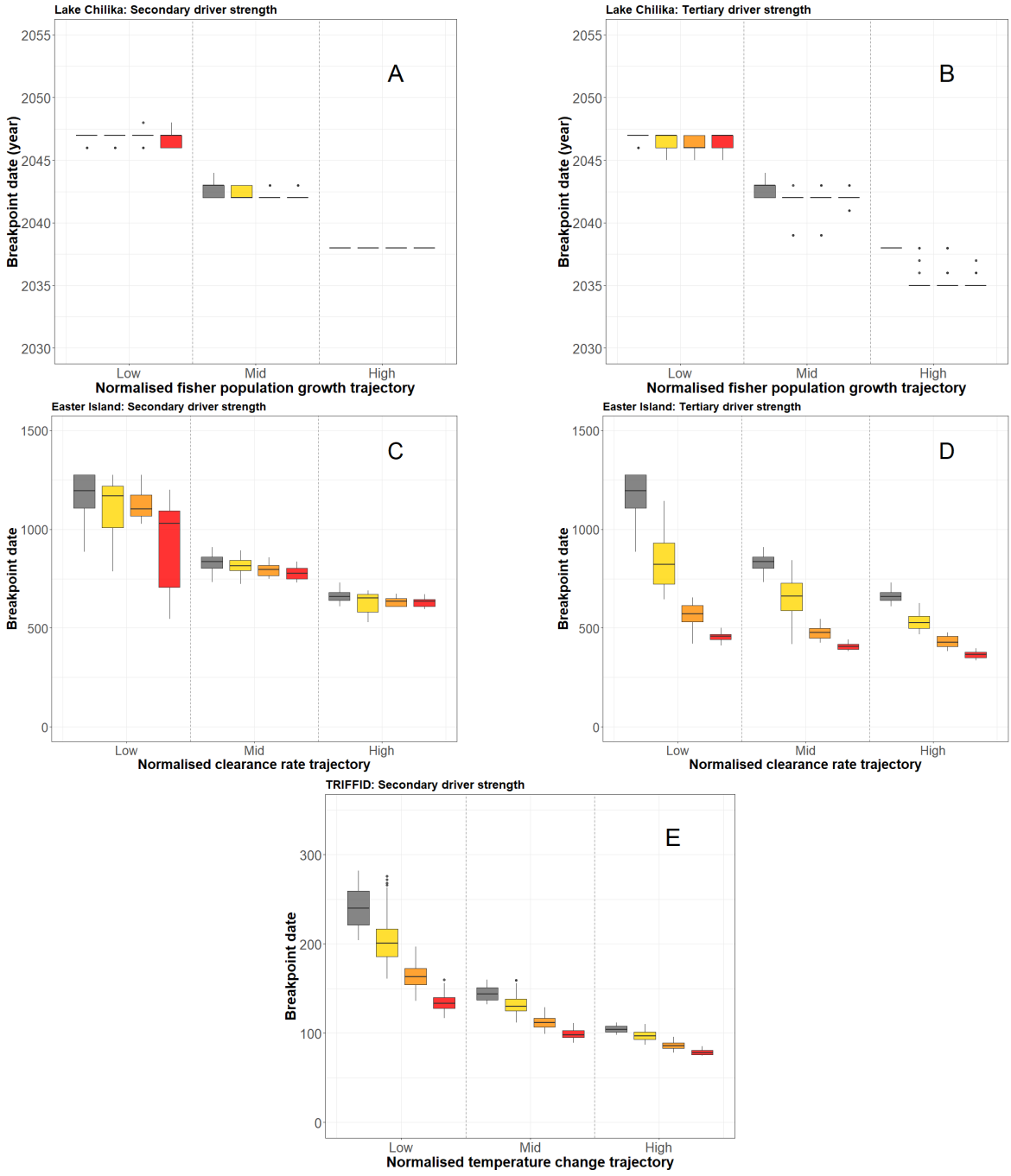

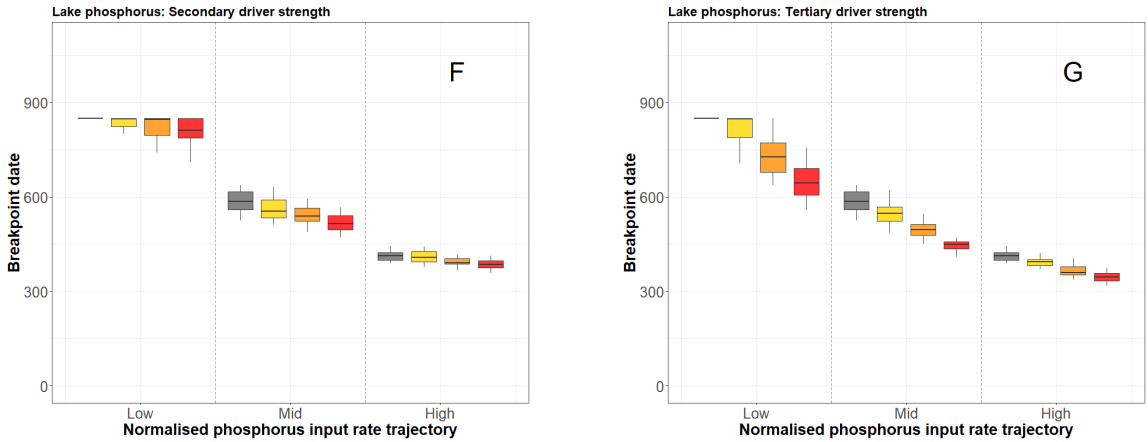

Figure S2-1: The distribution of breakpoint dates along the range of primary slow driver trajectories in each of the models, with the additional effects of the secondary and tertiary drivers in each model disaggregated. *As in the main manuscript (i.e., Figures 2-4), the normalised primary driver trajectories are apportioned into three discrete ranges: 'low' – 0.25-0.35, 'mid' – 0.45-0.55, and 'high' – 0.65-0.75. The left column shows the combined effects of the primary plus secondary drivers in each model, and the right column shows the combined effects of the primary plus tertiary drivers in each model. In line with the primary drivers, the secondary and tertiary drivers are apportioned into the same normalised trajectory ranges: 'low' – 0.25-0.35 (yellow), 'mid' – 0.45-0.55 (orange), and 'high' – 0.65-0.75 (red). Subplots: (A-B) Lake Chilika model, primary slow driver: fisher population growth, secondary driver: climate change, tertiary driver: fish price; (C-D) Easter Island model, primary slow driver = tree clearance, secondary driver: agricultural carrying capacity, tertiary driver: tree mortality; (E) TRIFFID model, primary slow driver: temperature change, secondary driver: disturbance rate; (F-G) Lake phosphorus model, primary slow driver: phosphorus external input, secondary driver: phosphorus recycling rate, tertiary driver: phosphorus sedimentation rate. Model timestep units: Lake Chilika, Easter Island and TRIFFID run in years; timesteps in Lake phosphorus are unitless. Boxplot dimensions are as Figure 2. The number of simulations (n) underpinning each primary driver trajectory range (i.e., low, middle, and high) in each of the above subplots are as follows: (A) 160, 173, and 160; (B) 158, 167 and 156; (C) 256, 235 and 233; (D) 281, 283 and 274; (E) 802, 800 and 815; (F) 128, 154, and 148; (G) 281, 283 and 274.*

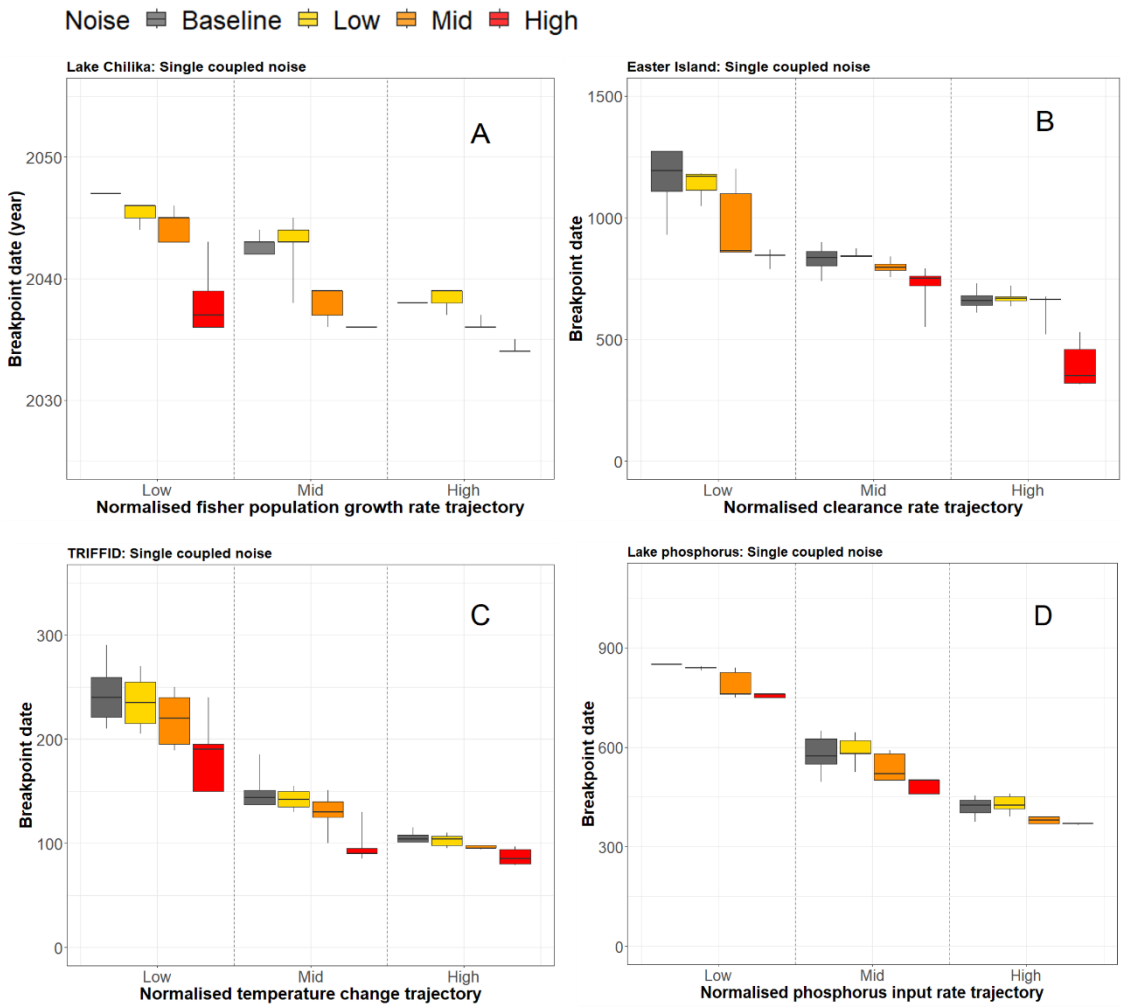

Figure S2-2: The relationship between the breakpoint date and the primary slow driver (grey) for varying levels of coupled noise in the primary driver (σ), where normalised σ values ≤ 0.333 signify 'low noise' (yellow), normalised σ values > 0.333 and ≤ 0.666 signify 'mid noise' (orange), and normalised σ values > 0.666 signify 'high noise' (red) (Methods Section 2.3). *As in the main manuscript (i.e., Figures 2-4), the normalised primary driver trajectories are apportioned into three discrete ranges: 'low' – 0.25-0.35, 'mid' – 0.45-0.55, and 'high' – 0.65-0.75. Subplots: (A) Lake Chilika model outputs, primary slow driver: fisher population growth; (B) Easter Island model outputs, primary slow driver = tree clearance; (C) TRIFFID model outputs, primary slow driver = temperature change; (D) Lake phosphorus model outputs, primary slow driver = phosphorus input. Model timestep units are the same as in Figure S2-1. Boxplot dimensions are as Figure 2. The number of simulations (n) underpinning each primary driver trajectory range (i.e., low, middle, and high) in each of the subplots are detailed in Table S3-1.*

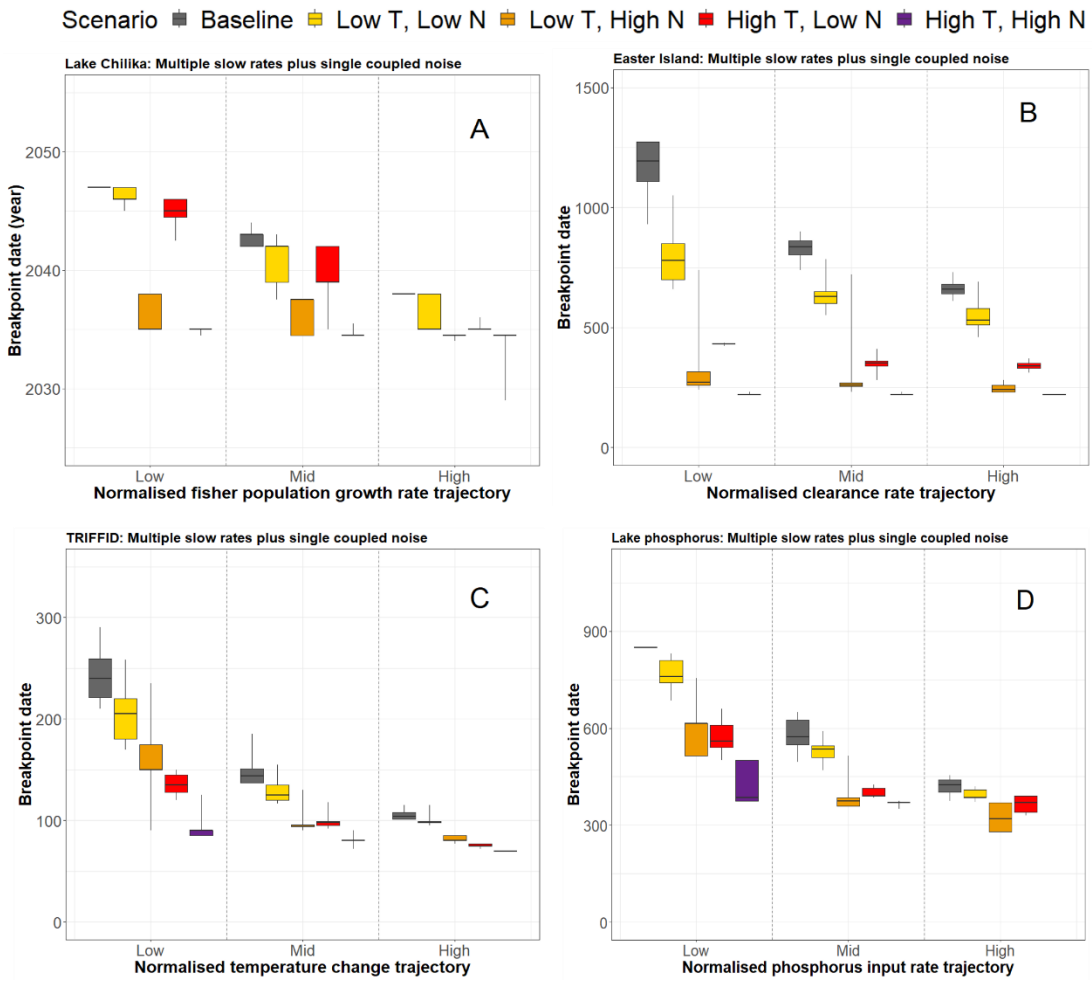

Figure S2-3: The relationship between the breakpoint date and the primary slow driver (grey) when weak (normalised T values ≤ 0.333) and strong (normalised T values > 0.666) multiple driver trajectories are combined with weak (normalised σ values ≤ 0.333) and strong (normalised σ values > 0.666) coupled noise (T = trajectory, N = noise). *As in the main manuscript (i.e., Figures 2-4), the normalised primary driver trajectories are apportioned into three discrete ranges: 'low' – 0.25-0.35, 'mid' – 0.45-0.55, and 'high' – 0.65-0.75. Subplots: (A) the Lake Chilika model , primary slow driver = fisher population growth, additional driver: climate change and fish price; (B) the Easter Island model, primary slow driver = tree clearance, additional drivers: agricultural carrying capacity and tree mortality; (C) the TRIFFID model, primary slow driver = temperature change, additional driver: disturbance rate; (D) the lake phosphorus model, primary slow driver = phosphorus, additional drivers: phosphorus recycling rate, phosphorus sedimentation rate. Model timestep units are the same as in Figure S2-1. Boxplot dimensions are as Figure 2. The number of simulations (n) underpinning each primary driver trajectory range (i.e., low, middle, and high) in each of the above subplots are detailed in Table S3-1.*

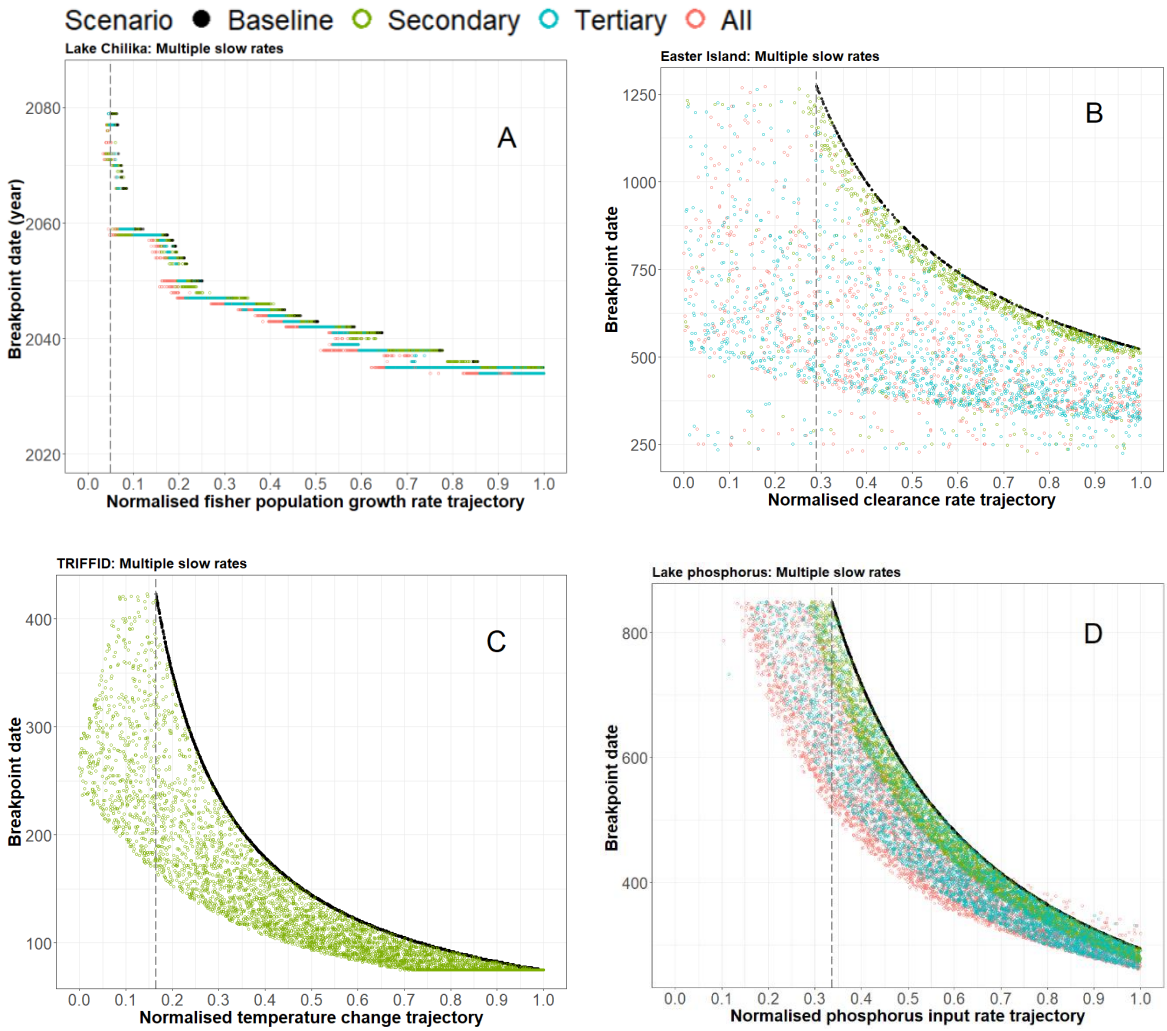

Figure S2-4: Scatter plots depicting the raw data producing the boxplots in Figure 2 of the main manuscript. *The dashed grey vertical line represents the weakest primary driver value associated with an ATDC in each plot. Subplots: (A) Lake Chilika model outputs, primary slow driver: fisher population growth; (B) Easter Island model outputs, primary slow driver = tree clearance; (C) TRIFFID model outputs, primary slow driver = temperature change; (D) Lake phosphorus model outputs, primary slow driver = phosphorus input. Model timestep units are the same as in Figure S2-1.*

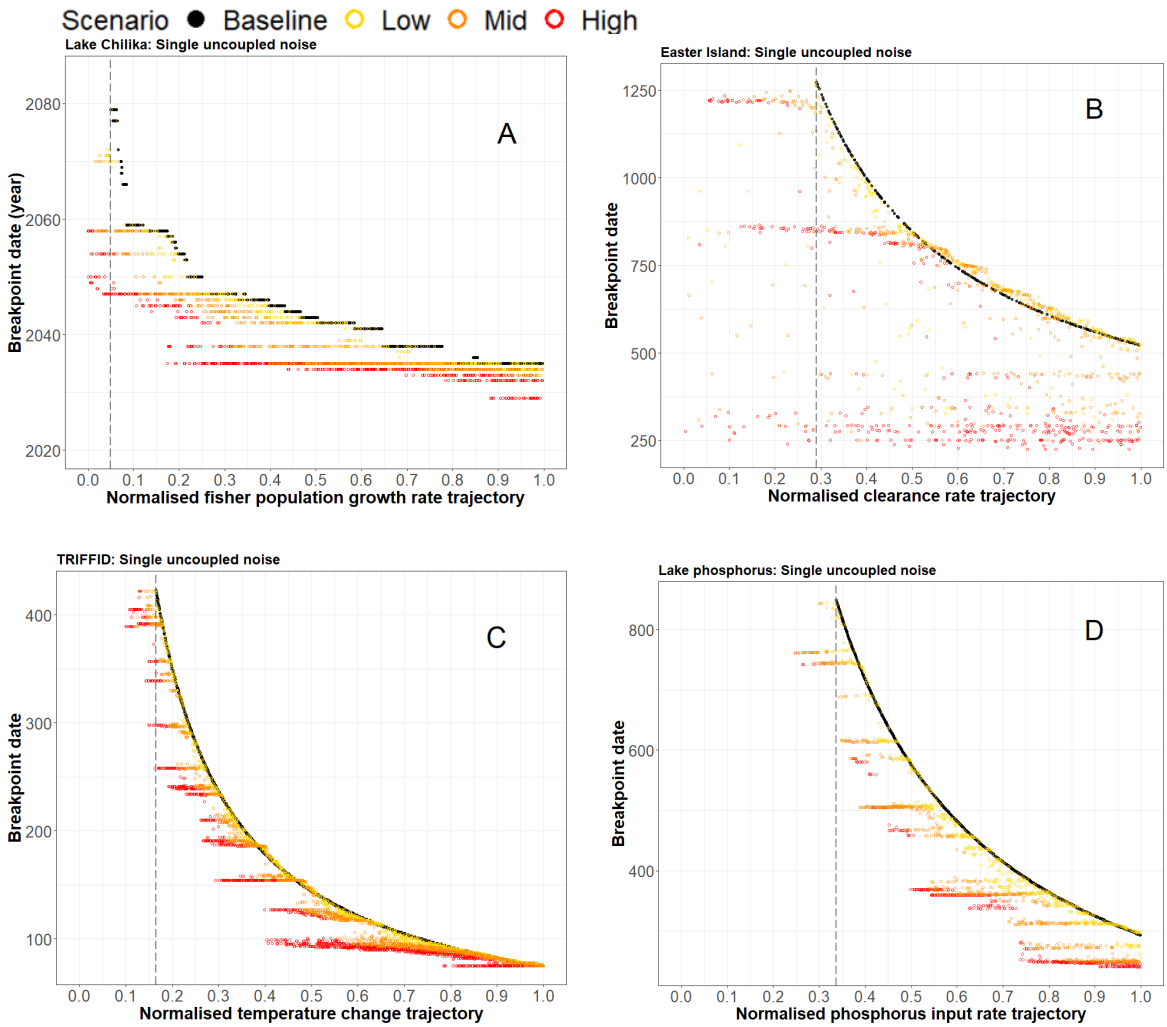

Figure S2-5: Scatter plots depicting the raw data producing the boxplots in Figure 3 of the main manuscript. *The dashed grey vertical line represents the weakest primary driver value associated with an ATDC in each plot. Subplots: (A) Lake Chilika model outputs, primary slow driver: fisher population growth; (B) Easter Island model outputs, primary slow driver = tree clearance; (C) TRIFFID model outputs, primary slow driver = temperature change; (D) Lake phosphorus model outputs, primary slow driver = phosphorus input. Model timestep units are the same as in Figure S2-1.*

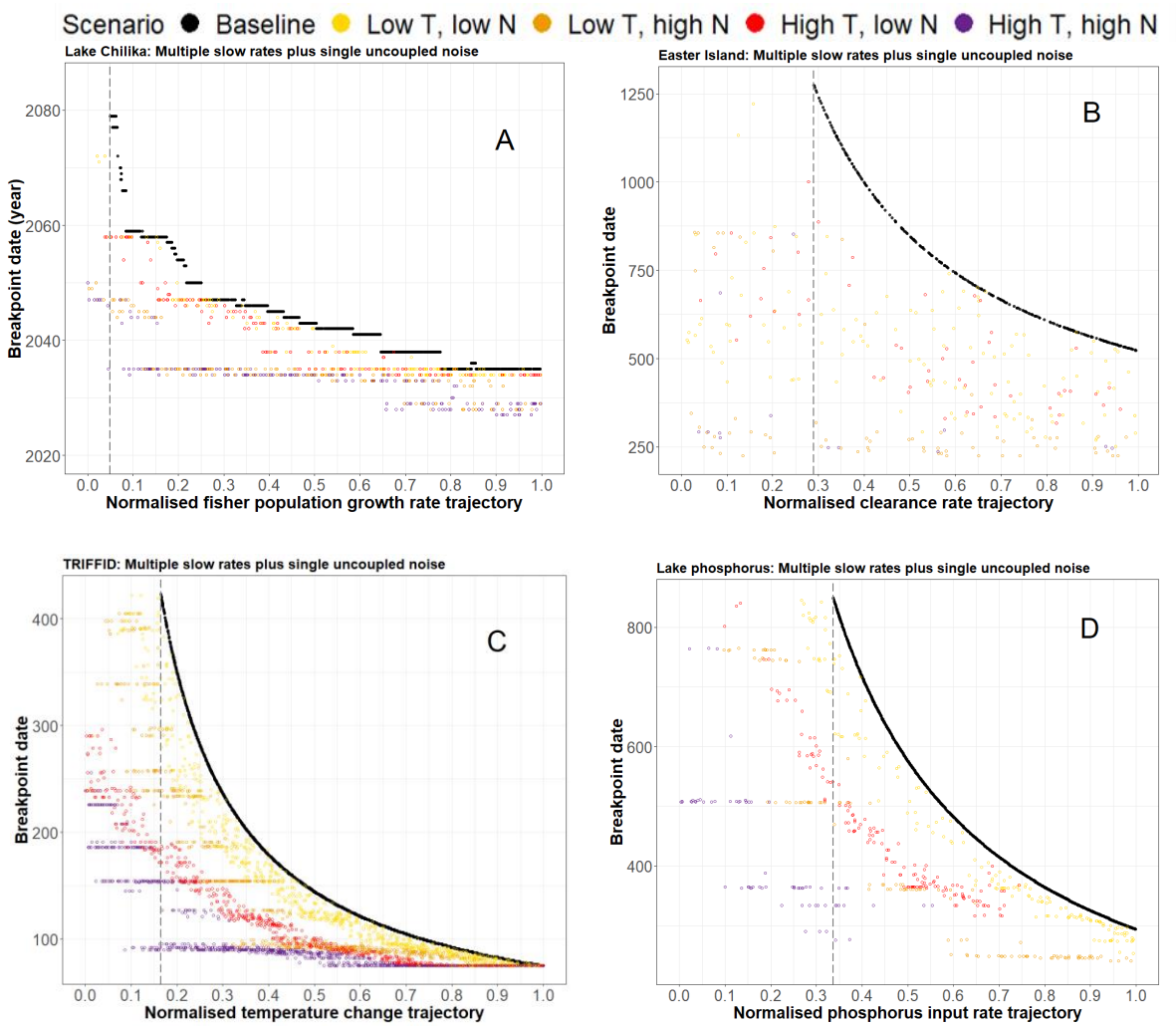

Figure S2-6: Scatter plots depicting the raw data producing the boxplots in Figure 4 of the main manuscript. *The dashed grey vertical line represents the weakest primary driver value associated with an ATDC in each plot. Subplots: (A) Lake Chilika model outputs, primary slow driver: fisher population growth; (B) Easter Island model outputs, primary slow driver = tree clearance; (C) TRIFFID model outputs, primary slow driver = temperature change; (D) Lake phosphorus model outputs, primary slow driver = phosphorus input. Model timestep units are the same as in Figure S2-1.*

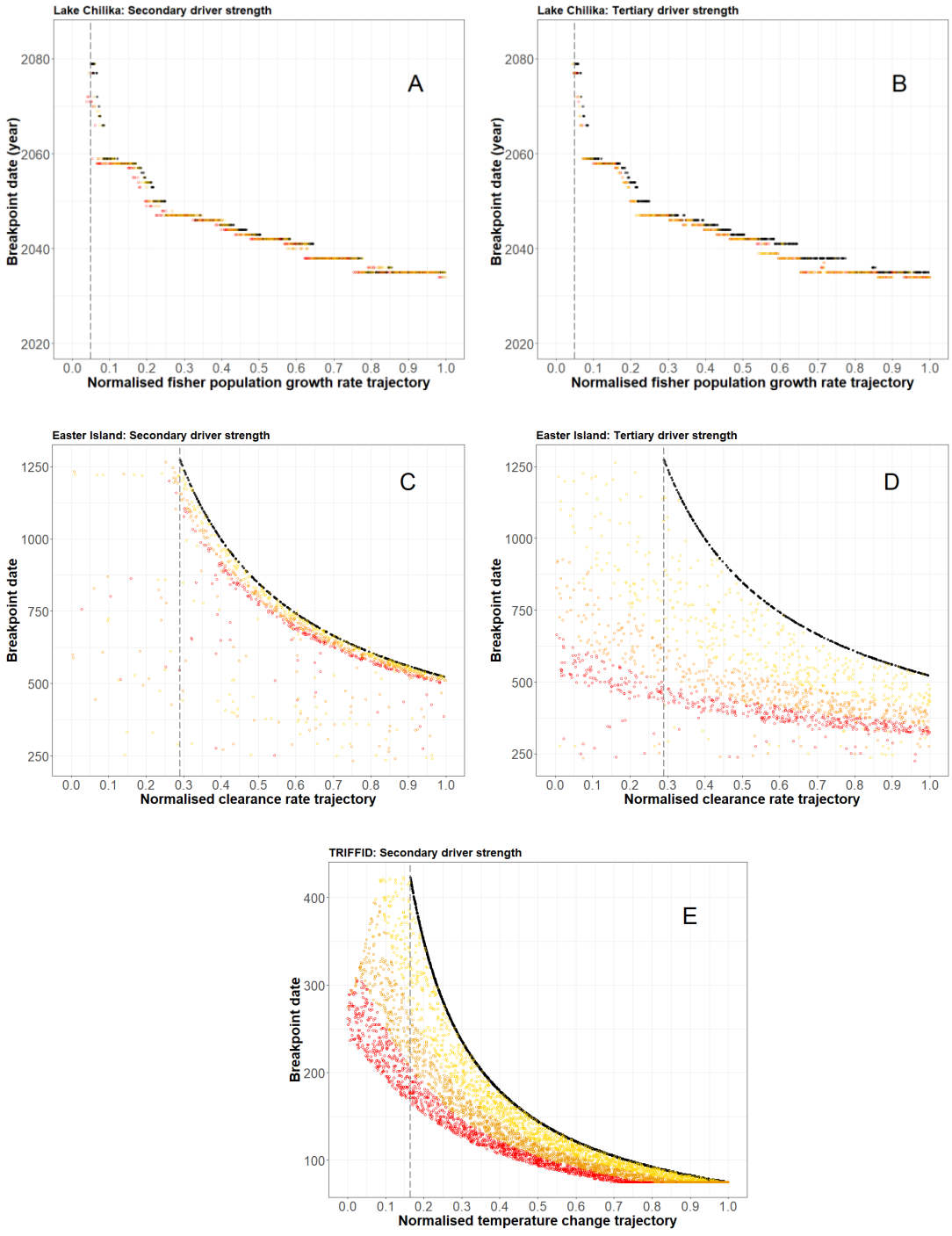
Lake Chilika: Secondary driver strength
A
Breakpoint date (year)
2080
2060
2040
2020
0.0 0.1 0.2 0.3 0.4 0.5 0.6 0.7 0.8 0.9 1.0
Normalised fisher population growth rate trajectory
Lake Chilika: Tertiary driver strength
B
Breakpoint date (year)
2080
2060
2040
2020
0.0 0.1 0.2 0.3 0.4 0.5 0.6 0.7 0.8 0.9 1.0
Normalised fisher population growth rate trajectory
Easter Island: Secondary driver strength
C
Breakpoint date
1250
1000
750
500
250
0.0 0.1 0.2 0.3 0.4 0.5 0.6 0.7 0.8 0.9 1.0
Normalised clearance rate trajectory
Easter Island: Tertiary driver strength
D
Breakpoint date
1250
1000
750
500
250
0.0 0.1 0.2 0.3 0.4 0.5 0.6 0.7 0.8 0.9 1.0
Normalised clearance rate trajectory
TRIFFID: Secondary driver strength
E
Breakpoint date
400
300
200
100
0.0 0.1 0.2 0.3 0.4 0.5 0.6 0.7 0.8 0.9 1.0
Normalised temperature change trajectory

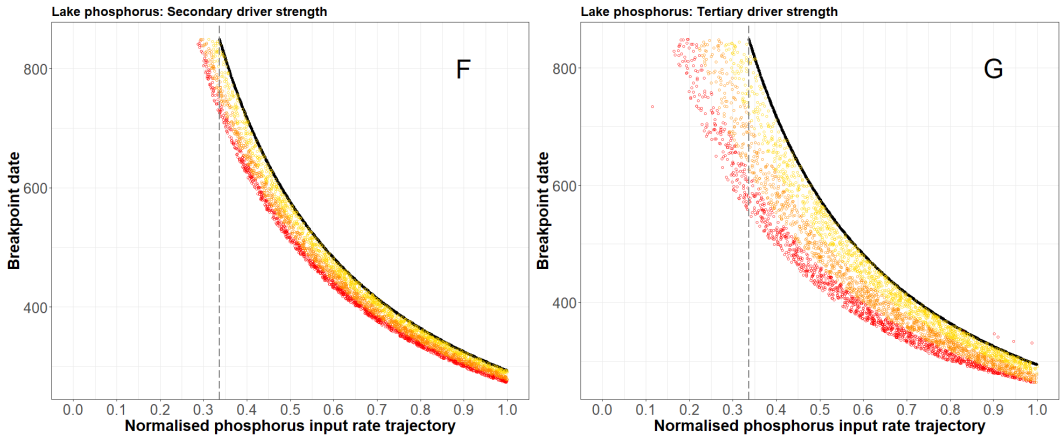

Figure S2-7: Scatter plots depicting the raw data producing the boxplots in Figure S2-1. The dashed grey vertical line represents the weakest primary driver value associated with an ATDC in each plot. *As per Figure S2-1, the left column shows the combined effects of the primary plus secondary drivers in each model, and the right column shows the combined effects of the primary plus tertiary drivers in each model Subplots: (A-B) Lake Chilika model, primary slow driver: fisher population growth, secondary driver: climate change, tertiary driver: fish price; (C-D) Easter Island model, primary slow driver = tree clearance, secondary driver: agricultural carrying capacity, tertiary driver: tree mortality; (E) TRIFFID model, primary slow driver: temperature change, secondary driver: disturbance rate; (F-G) Lake phosphorus model, primary slow driver: phosphorus external input, secondary driver: phosphorus recycling rate, tertiary driver: phosphorus sedimentation rate. Model timestep units are the same as in Figure S2-1.*

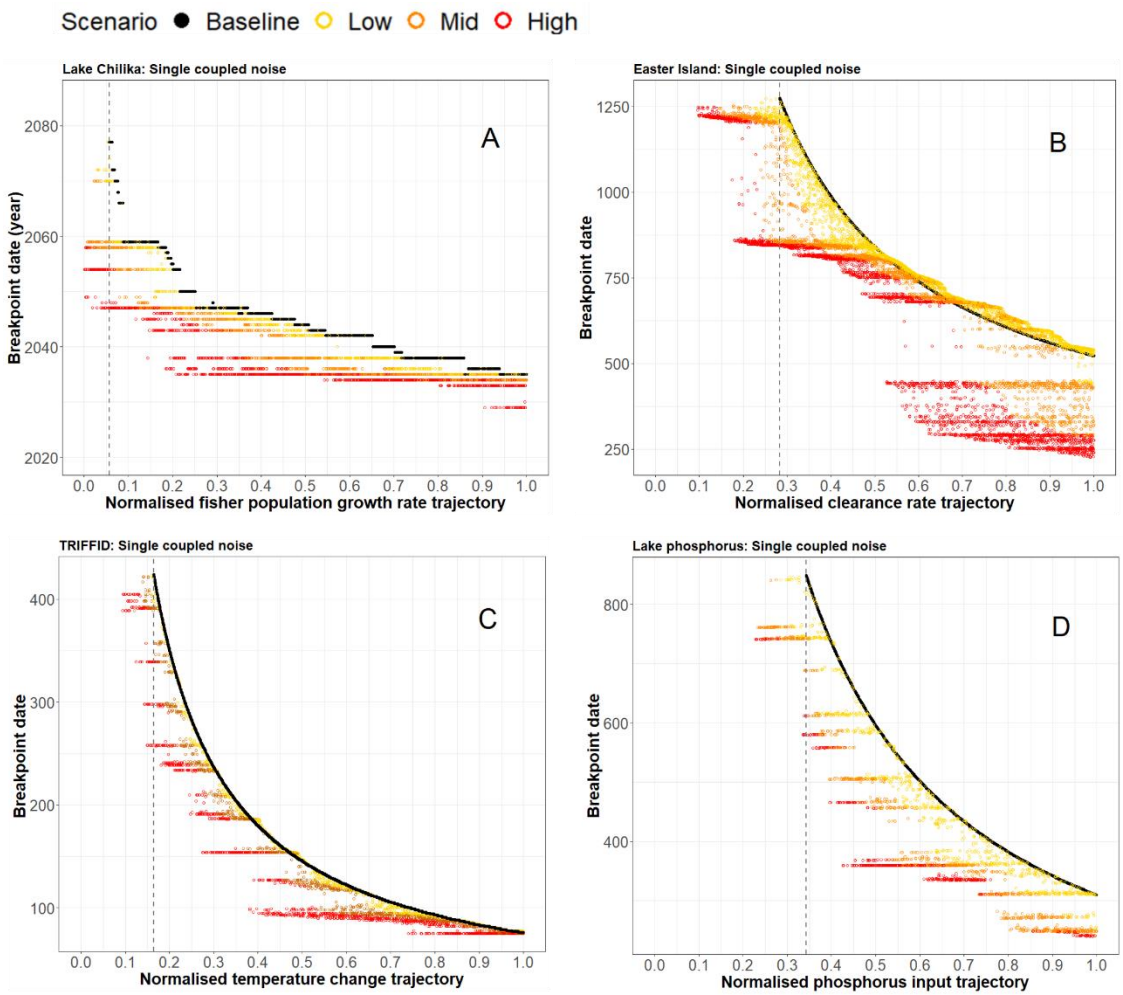

Figure S2-8: Scatter plots depicting the raw data producing the boxplots in Figure S2-2. *The dashed grey vertical line represents the weakest primary driver value associated with an ATDC in each plot. Subplots: (A) Lake Chilika model outputs, primary slow driver: fisher population growth; (B) Easter Island model outputs, primary slow driver = tree clearance; (C) TRIFFID model outputs, primary slow driver = temperature change; (D) Lake phosphorus model outputs, primary slow driver = phosphorus input. Model timestep units are the same as in Figure S2-1.*

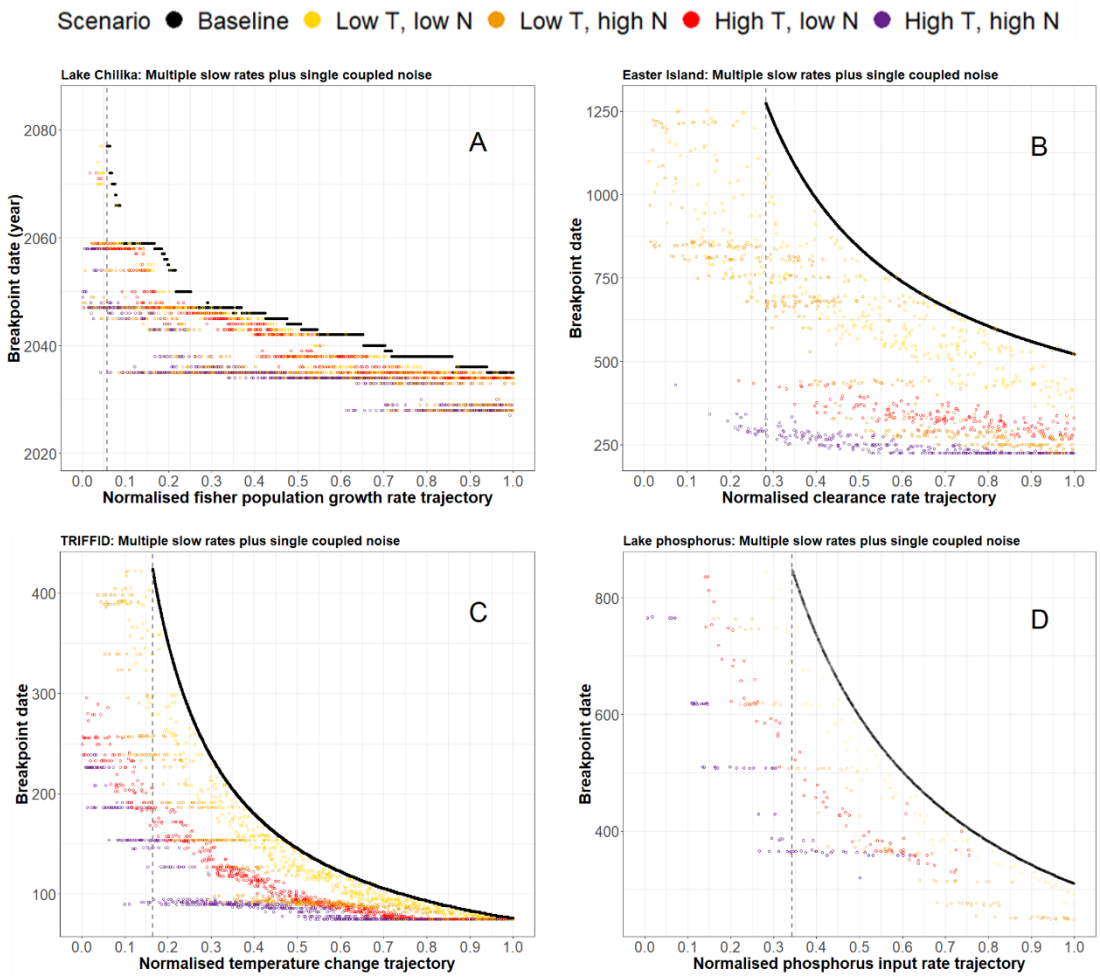

Figure S2-9: Scatter plots depicting the raw data producing the boxplots in Figure S2-3. *The dashed grey vertical line represents the weakest primary driver value associated with an ATDC in each plot. Subplots: (A) Lake Chilika model outputs, primary slow driver: fisher population growth; (B) Easter Island model outputs, primary slow driver = tree clearance; (C) TRIFFID model outputs, primary slow driver = temperature change; (D) Lake phosphorus model outputs, primary slow driver = phosphorus input. Model timestep units are the same as in Figure S2-1.*

Table S2-1: Abrupt threshold-dependent changes (ATDCs) triggered by additional drivers below the minimum driver strengths required to collapse the system if only a single driver were in effect.

Model	**Number of model runs which tipped at primary driver strengths below the minimum observed to cause an ATDC if only a single driver were in effect**				**Total runs across all scenarios which tipped**
	Additional secondary driver	**Additional tertiary driver**	**Additional secondary and tertiary drivers**	**Total (%)**	
Lake Chilika	55	45	133	233 (1.21%)	19,208
Easter Island	7	1018	983	2008 (14.8%)	13,574
TRIFFID	1410	NA	NA	1410 (7.70%)	18,319
Lake phosphorus	306	669	1895	2870 (12.3%)	23,270

Table S2-2: Abrupt threshold-dependent changes (ATDCs) triggered by additional uncoupled noise below the minimum driver strengths required to collapse the system if only a single driver were in effect, *where normalised σ values ≤ 0.333 signify 'low noise', normalised σ values > 0.333 and ≤ 0.666 signify 'mid noise', and normalised σ values > 0.666 signify 'high noise'.*

Model	**Number of model runs which tipped at primary driver strengths below the minimum observed to cause an ATDC if only a single driver were in effect**				**Total runs across all scenarios which tipped**
	Low noise	**Mid noise**	**High noise**	**Total (%)**	
Lake Chilika	28	78	85	191 (2.50%)	7643
Easter Island	24	93	291	408 (6.57%)	6209
TRIFFID	22	103	221	346 (2.02%)	17,126
Lake phosphorus	8	40	79	127 (2.63%)	4831

Table S2-3: Abrupt threshold-dependent changes (ATDCs) triggered by additional coupled noise below the minimum driver strengths required to collapse the system if only a single driver were in effect, *where normalised σ values ≤ 0.333 signify 'low noise', normalised σ values > 0.333 and ≤ 0.666 signify 'mid noise', and normalised σ values > 0.666 signify 'high noise'.*

Model	**Number of model runs which tipped at primary driver strengths below the minimum observed to cause an ATDC if only a single driver were in effect**				**Total runs across all scenarios which tipped**
	Low noise	**Mid noise**	**High noise**	**Total (%)**	
Lake Chilika	25	80	86	191 (2.48%)	7691
Easter Island	85	347	566	998 (9.69%)	10,302
TRIFFID	3	42	88	133 (1.30%)	10,244
Lake phosphorus	36	129	28	193 (3.98%)	4849

Table S2-4: Abrupt threshold-dependent changes (ATDCs) triggered below the minimum driver strengths required to collapse the system if only a single driver were in effect when weak (normalised T values ≤ 0.333) and strong (normalised T values > 0.666) multiple driver trajectories are combined with weak (normalised σ values ≤ 0.333) and strong (normalised σ values > 0.666) uncoupled noise (T = trajectory, N = noise).

Model	**Number of model runs which tipped at primary driver strengths below the minimum observed to cause an ATDC if only a single driver were in effect**					**Total runs across all scenarios which tipped**
	Low T, Low N	**Low T, High N**	**High T, Low N**	**High T, High N**	**Total (%)**	
Lake Chilika	17	25	12	26	80 (1.73%)	4619
Easter Island	62	100	2	118	282 (7.45%)	3784
TRIFFID	142	208	284	347	981 (6.64%)	14,775
Lake phosphorus	26	59	103	127	315 (8.92%)	3533

Table S2-5: Abrupt threshold-dependent changes (ATDCs) triggered below the minimum driver strengths required to collapse the system if only a single driver were in effect when weak (normalised T values ≤ 0.333) and strong (normalised T values > 0.666) multiple driver trajectories are combined with weak (normalised σ values ≤ 0.333) and strong (normalised σ values > 0.666) coupled noise (T = trajectory, N = noise).

Model	**Number of model runs which tipped at primary driver strengths below the minimum observed to cause an ATDC if only a single driver were in effect**					**Total runs across all scenarios which tipped**
	Low T, Low N	**Low T, High N**	**High T, Low N**	**High T, High N**	**Total (%)**	
Lake Chilika	28	32	23	55	138 (2.67%)	6083
Easter Island	83	92	2	24	201 (6.04%)	3330
TRIFFID	43	73	104	111	331 (3.50%)	9477
Lake phosphorus	7	21	30	42	100 (3.44%)	2911

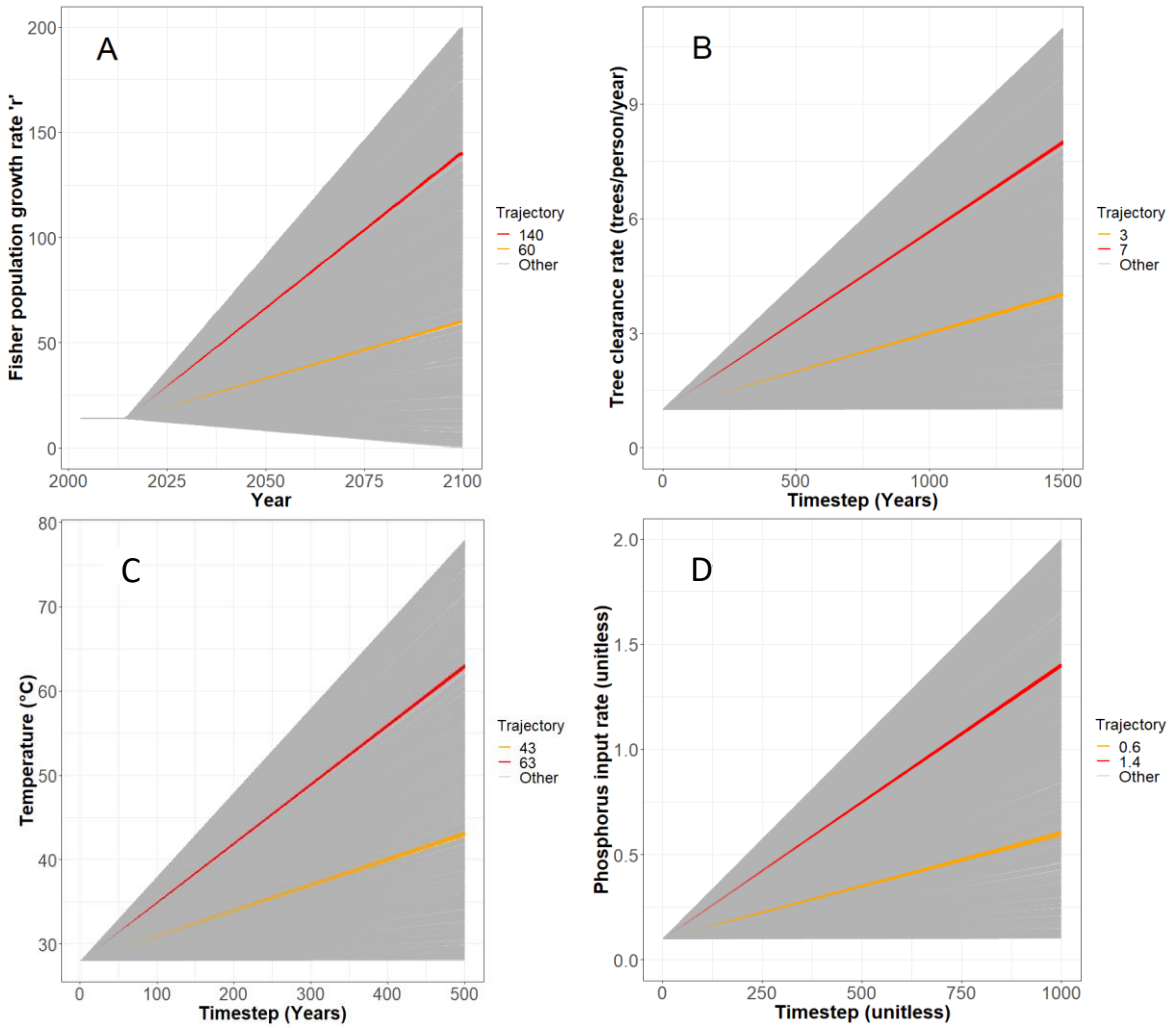

Figure S3-1: The future scenario funnels of the four primary (baseline) slow trajectories over the course of their respective model horizons. *Subplots clockwise from top-left: (A) array of linear changes in the fisher population growth rate 'r' (net difference between the crude birth and crude death rates of the fisher population) in the Lake Chilika fishery model; (B) array of linear changes in the tree clearance rate in the Easter Island model; (C) array of linear changes in the local temperature in the TRIFFID model; (D) array of linear changes in the phosphorus input rate in the Lake phosphorus model. As described in Methods Section 2.3, the drivers start at their default values before moving along a randomly selected future trajectory (Table S2-1). The gradient trajectories representing 30% and 70% of the maximum possible trajectories have been identified in orange and red, respectively. The same approach is also used for all secondary and tertiary drivers, evolving along randomly selected linear gradients between 'no change from default' and 'maximum change' by the model horizon.*

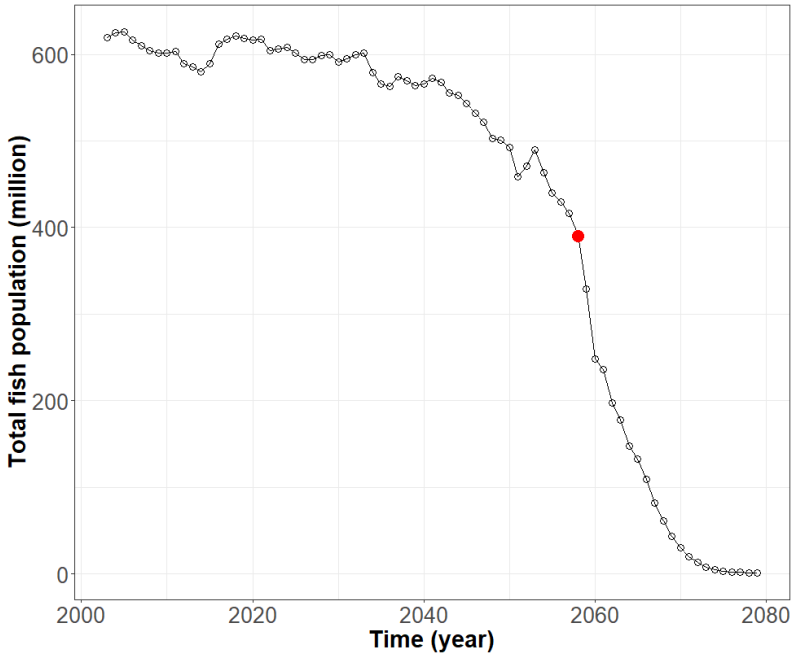

Figure S3-2: Fish population timeseries from an example Lake Chilika model simulation, where the 'strucchange' breakpoint function identifies the breakdate as 2058 (red dot). *Using this method, timesteps either side of the breakdate are considered to be in alternative regimes (see SI-4 for alternative threshold definitions).*

Table S3-1: The number of model simulations constituting each experiment and scenario, as plotted in Figures 2 to 4 and Figure S2-1 to S2-3. *Each of the model runs were identified to have gone through an abrupt threshold-dependent change (ATDC), as per the methodology detailed in Methods Section 3.1 and 3.2. T = Trajectory, N = Noise*.

		Experiment 2: Multiple slow drivers			**Experiment 3a: Single slow driver plus uncoupled noise**			**Experiment 4a: Multiple slow drivers plus uncoupled noise**			
Model	**Experiment 1: Baseline**	*Secondary*	*Tertiary*	*All*	*Low*	*Medium*	*High*	*Low T, Low N*	*Low T, High N*	*High T, Low N*	*High T, High N*
Lake Chilika	3016	4603	4561	7028	1429	1602	1596	409	388	398	408
Easter Island	2118	2097	4769	4590	1255	1297	1539	468	394	231	573
TRIFFID	6833	11486			3354	3393	3546	2028	1777	1845	2292
Lake phosphorus	2556	5425	5744	9545	762	733	780	260	283	257	177
					Experiment 3b: Single slow driver plus coupled noise			**Experiment 4b: Multiple slow drivers plus coupled noise**			
					Low	*Medium*	*High*	*Low T, Low N*	*Low T, High N*	*High T, Low N*	*High T, High N*
Lake Chilika	3016				1429	1602	1596	760	738	759	810
Easter Island	2118				2530	2603	3051	340	405	172	295
TRIFFID	6833				1088	1095	1228	614	643	671	716
Lake phosphorus	9545				824	945	524	96	110	83	66

Table S3-2: Range of parameter values driving the trajectory changes and addition of noise (σ) across the four experiment types (*Methods Section 2.1*) in each of the four models. *The numbers in superscripts denote the corresponding experiment type where the given scenario ranges are active. Experiment #1[1]: change in the trajectory of the primary driver only; Experiment #2[2]: changes in the trajectories of the primary driver and additional driver trajectories; Experiment 3[3]: changes in the trajectories of the primary driver and the addition of noise to the primary driver; Experiment #4[4]: change in the trajectories of the primary driver and additional driver trajectories, plus the addition of noise to the primary driver. Experiments #3 and #4 here include both coupled and uncoupled noise.*

Model	External variable	Unit	Default value	Range of slow driver change trajectories	Noise (σ) range
Lake Chilika	Fisher population growth rate 'r'	Unitless	14	-14 – 186 [1,2,3,4]	0 – 100 [3,4]
	Annual rainfall total change (2081-2100 relative to 1986-2005)	%	0	0 – 30 [2,4]	0 [1,2,3,4]
	Annual mean temperature change (2081-2100 relative to 1986-2005)	ºC	0	0 – 4.5 [2,4]	0 [1,2,3,4]
	Change in fish price per unit	INR/kg	0	0 – 2550 [2,4]	0 [1,2,3,4]
Easter Island	Tree clearance	Trees/person/ year	1	0 – 10 [1,2,3,4]	0 – 20 [3,4]
	Agricultural carrying capacity	Persons	1200	0 – 6200 [2,4]	0 [1,2,3,4]
	Mortality rate of trees	Trees/year	0.01	0 – 0.1 [2,4]	0 [1,2,3,4]
Lake phosphorus	Phosphorus input	Unitless	0.1	0 – 2 [1,2,3,4]	0 – 0.5 [3,4]
	Recycling rate	Unitless	1	0 – 3 [2,4]	0 [1,2,3,4]
	Sedimentation	Unitless	1	-0.5 – 0 [2,4]	0 [1,2,3,4]
TRIFFID	Local temperature	ºC	28	0 – 50 [1,2,3,4]	0 – 10 [3,4]
	Disturbance rate	Trees/year	0.2	0 – 2 [2,4]	0 [1,2,3,4]

SI-4: Alternative Threshold Definitions for Identification of ATDCs

Introduction and methods

As described in Methods Section 3.2, the results presented in Figures 2 to 4 are based on the optimal breakpoint function of Zeileis *et al.*[9], which finds the most significant deviation from stability in classical regression models (i.e. where regressions coefficients shift from one stable regime to another). However, numerous possible breakpoint methods can be used to identify ATDCs[4]. To ensure our results were robust to the breakpoint method used, we reanalysed the first 10,000 simulations across all four models using two further threshold definitions based on the classification of boundary types defined by Dearing *et al.*[4] (i.e. 'linear' and 'non-linear', with the breakpoint function presented in the main manuscript representing an 'abrupt type-3 threshold').

Alternative Method 1: Type 1a thresholds – Environmental limits

Conceptualised as *"quantitative measures of the state of beneficial ecosystem processes that, once exceeded, significantly constrain conventional resource use"* (4; p.231), the first alternative method of defining the breakpoint date for the Lake Chilika, Easter Island and TRIFFID models is the first timestep beyond which the outcome variable falls beneath 20% of its initial value at model initialisation (i.e., timestep 0). As described in Methods Section 3.1, this demarcation is based upon the concept that fish stocks may be considered quantitatively collapsed once their biomass falls beneath 20% of the biomass needed to maintain sustainable yields[10,11]. Furthermore, as depicted in Figure 1 and described in Methods Section 3.1, this approach is already used to isolate simulations which collapse to a quantitatively different state, before the breakpoint function of Zeileis *et al.*[9] dates the timestep when outcome versus timestep regressions coefficients shift from one stable regime to another.

Given that lake phosphorus concentrations increase (rather than collapse), it is not suitable to apply the '20% of initial' environmental limit to the Lake phosphorus model. We define an alternative environmental limit based on Figure 2 of Carpenter[12], whereby the baseline model of lake eutrophication undergoes a regime shift once the lake water phosphorus concentration exceeds 1.3 (g/m^2). Therefore, for the Lake phosphorus simulations depicted in Figures S4-1 to S4-4, we define the breakpoint date as the first timestep that the outcome variable (i.e., lake water phosphorus concentration) is greater than 1.3 (g/m^2).

Alternative Method 2: Type 2a thresholds – Rate of change

Conceptualised as *"[a boundary]… where there is an unacceptable acceleration in a harmful effect or a decline in a beneficial ecosystem process"* (4; p.231), the second alternative method defines the threshold as the timestep corresponding to the highest change in the outcome variable over time. In practice, the first difference in the outcome timeseries is calculated for each simulation that reaches a quantitatively different state (i.e., as per Section 3.1), and the timestep within each simulation with the highest first difference value is taken as the threshold. This method is applied uniformly to all four models, as the first differencing approach is not sensitive to whether the outcome variable grows (in the case of Lake phosphorus) or collapses (in the case of Lake Chilika, Easter Island and TRIFFID).

Results

Alternative Method 1: Type 1a thresholds – Environmental limits

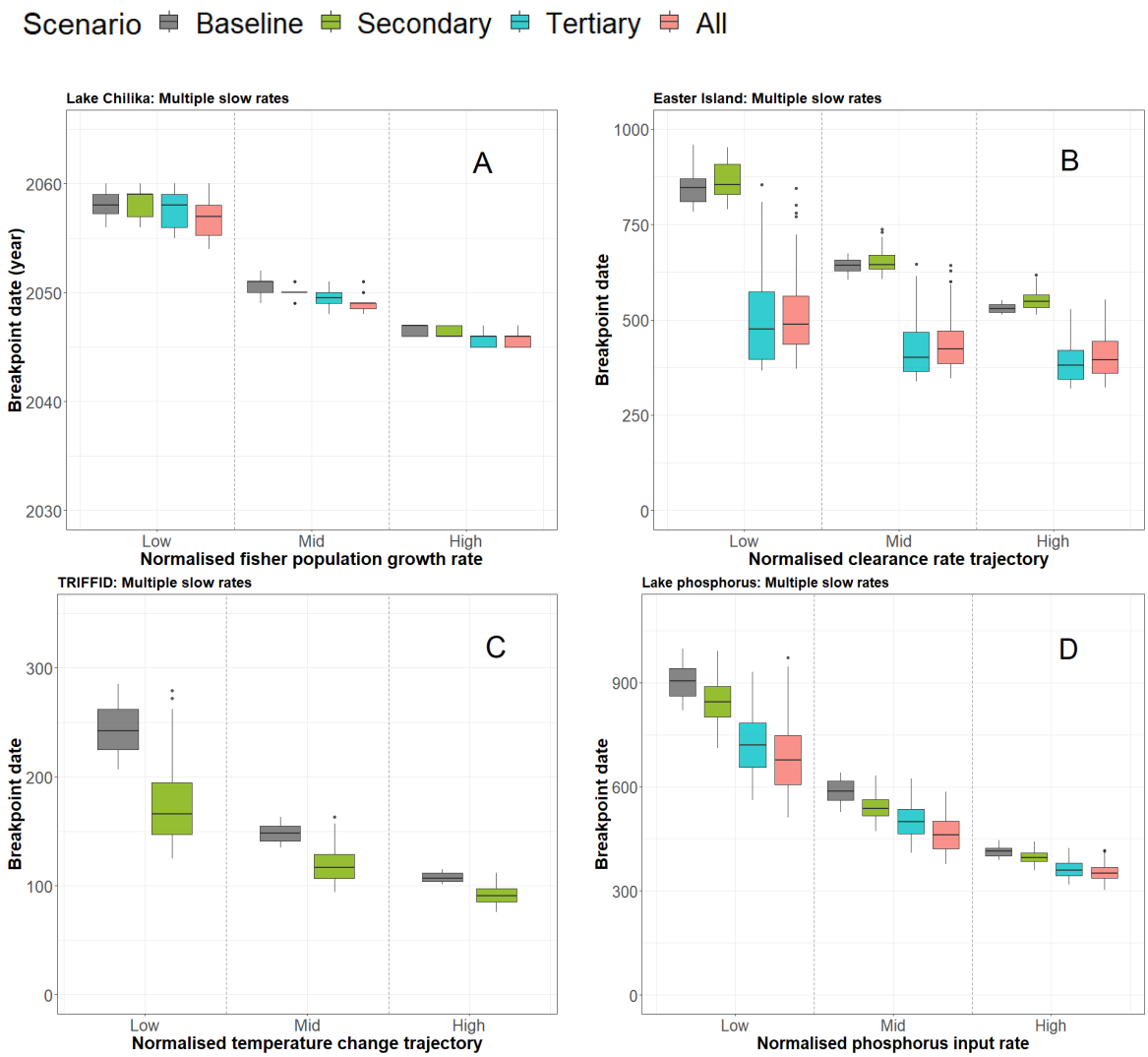

Figure S4-1: The relationship between the breakpoint date and the primary (baseline) slow driver for the individual (grey) and multiple (coloured) drivers, when the breakpoint date is defined by the first alternative method described above (Type 1a boundaries). *As in the main manuscript (i.e., Figures 2-4), the normalised primary driver trajectories are apportioned into three discrete ranges: 'low' – 0.25-0.35, 'mid' – 0.45-0.55, and 'high' – 0.65-0.75. For comparison with the main manuscript, this figure is the equivalent of Figure 2. Subplots: (A) Lake Chilika model, primary slow driver: fisher population growth, secondary driver: climate change, tertiary driver: fish price; (B) Easter Island model, primary slow driver = tree clearance, secondary driver: agricultural carrying capacity, tertiary driver: tree mortality; (C) TRIFFID model, primary slow driver: temperature change, secondary driver: disturbance rate; (D) Lake phosphorus model, primary slow driver: phosphorus external input, secondary driver: phosphorus recycling rate, tertiary driver: phosphorus sedimentation rate. Model timestep units are the same as in Figure S2-1. Boxplot dimensions are as Figure 2. The number of simulations (n) underpinning each primary driver trajectory range (i.e., low, middle, and high) in each of the above subplots are as follows: (A) 182, 220, and 203; (B) 315, 355, and 350; (C) 400, 410, and 394 ; (D) 398, 410, and 394.*

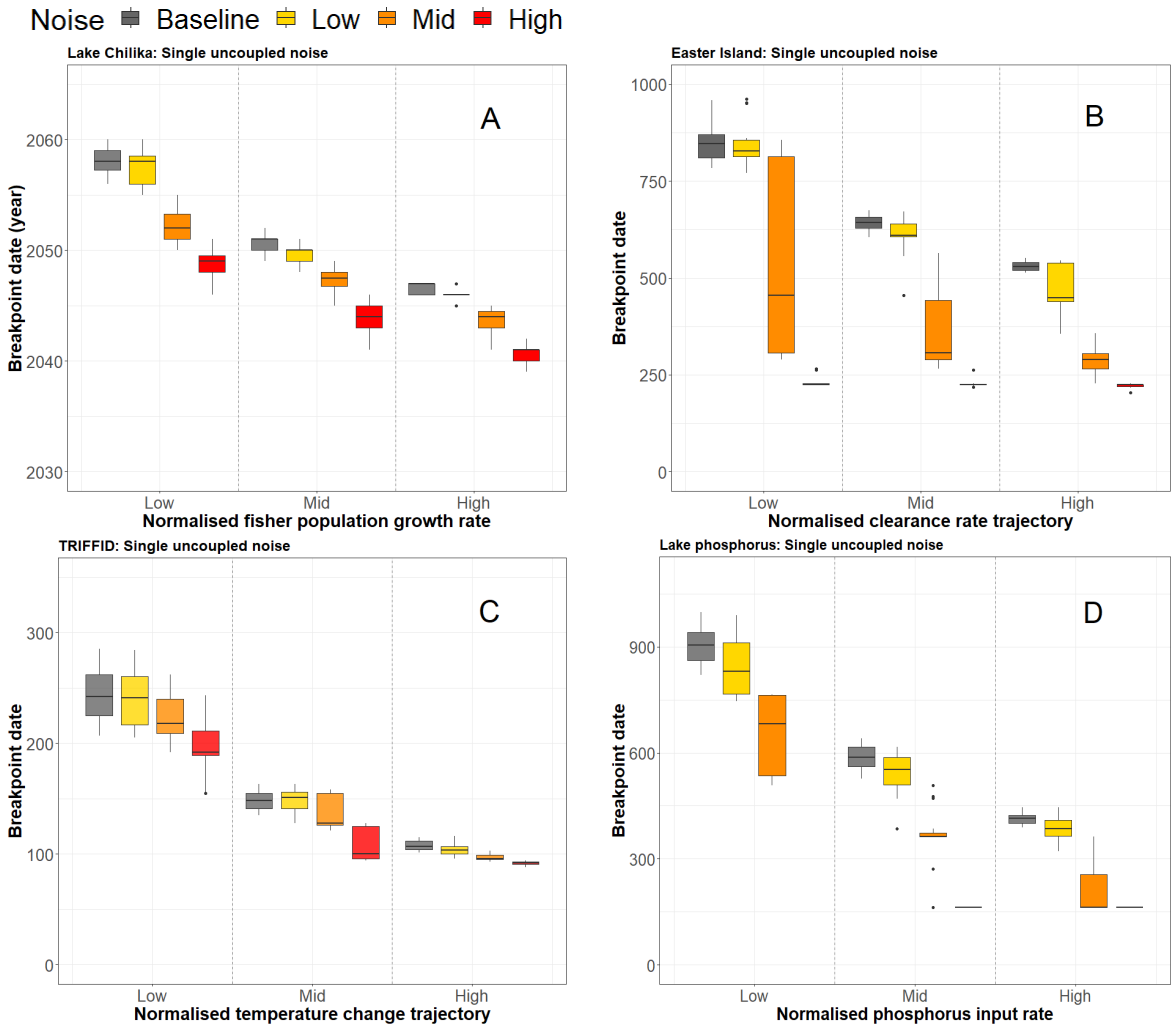

Figure S4-2: The relationship between the breakpoint date and the primary slow driver (grey) for varying levels of uncoupled noise in the primary slow driver (σ), where normalised σ values ≤ 0.333 signify 'low noise' (yellow), normalised σ values > 0.333 and ≤ 0.666 signify 'mid noise' (orange), and normalised σ values > 0.666 signify 'high noise' (red) (Methods Section 2.3). The breakpoint date is defined by the first alternative method described above (Type 1a boundaries). *As in the main manuscript (i.e., Figures 2-4), the normalised primary driver trajectories are apportioned into three discrete ranges: 'low' – 0.25-0.35, 'mid' – 0.45-0.55, and 'high' – 0.65-0.75. For comparison with the main manuscript, this figure is the equivalent of Figure 3. Subplots: (A) Lake Chilika model outputs, primary slow driver = fisher population growth; (B) Easter Island model outputs, primary slow driver = tree clearance; (C) TRIFFID model outputs, primary slow driver = temperature change; (D) Lake phosphorus model outputs, primary slow driver = phosphorus input. Model timestep units are the same as in Figure S2-1. Boxplot dimensions are as Figure 2. The number of simulations (n) underpinning each primary driver trajectory range (i.e., low, middle, and high) in each of the above subplots are as follows: (A) 76, 81, and 73; (B) 158, 167, and 156; (C) 403, 389, and 377; (D) 82, 128, and 133.*

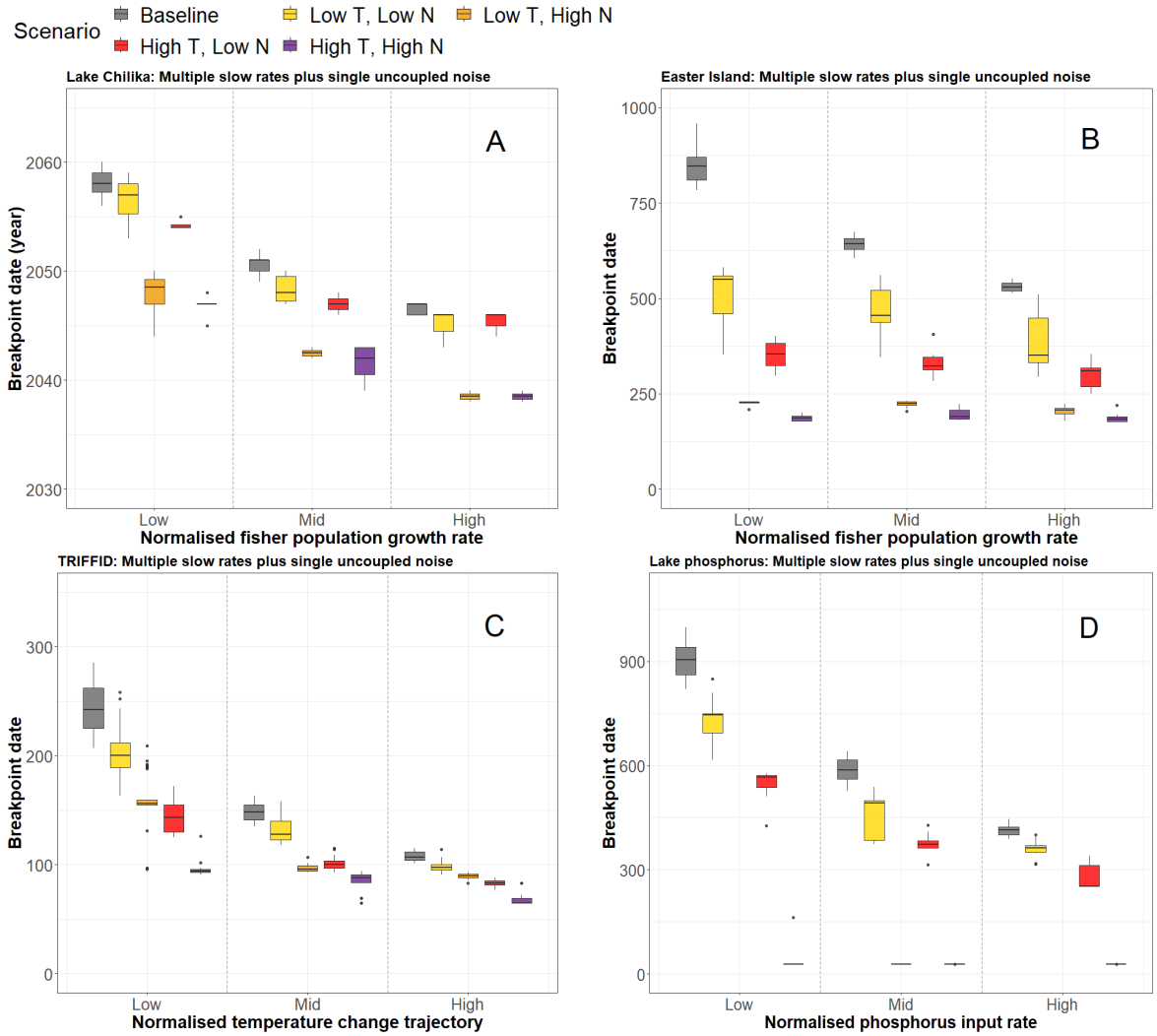

Figure S4-3: The relationship between the breakpoint date and the primary slow driver (grey) when weak (normalised T values ≤ 0.333) and strong (normalised T values > 0.666) multiple driver trajectories are combined with weak (normalised σ values ≤ 0.333) and strong (normalised σ values > 0.666) uncoupled noise (T = trajectory, N = noise). The breakpoint date is defined by the first alternative method described above (Type 1a boundaries). *As in the main manuscript (i.e., Figures 2-4), the normalised primary driver trajectories are apportioned into three discrete ranges: 'low' – 0.25-0.35, 'mid' – 0.45-0.55, and 'high' – 0.65-0.75. For comparison with the main manuscript, this figure is the equivalent of Figure 4. Subplots: (A) the Lake Chilika model, primary slow driver = fisher population growth, additional driver: climate change and fish price; (B) the Easter Island model, primary slow driver = tree clearance, additional drivers: agricultural carrying capacity and tree mortality; (C) the TRIFFID model, primary slow driver = temperature change, additional driver: disturbance rate; (D) the Lake phosphorus model, primary slow driver = phosphorus, additional drivers: phosphorus recycling rate, phosphorus sedimentation rate. Note, the first 10,000 simulations of the Lake phosphorus model (subplot D) did not produce any outcomes between the 0.25-0.35 and 0.65-0.75 primary driver ranges within the 'low trajectory, high noise' scenario. Model timestep units are the same as in Figure S2-1. Boxplot dimensions are as Figure 2. The number of simulations (n) underpinning each primary driver trajectory range (i.e., low, middle, and high) in each of the above subplots are as follows: (A) 45, 50, and 40; (B) 81, 102 and 96; (C) 333, 328, and 308; (D) 73, 89 and 82.*

Alternative Method 2: Type 2a thresholds – Rate of change

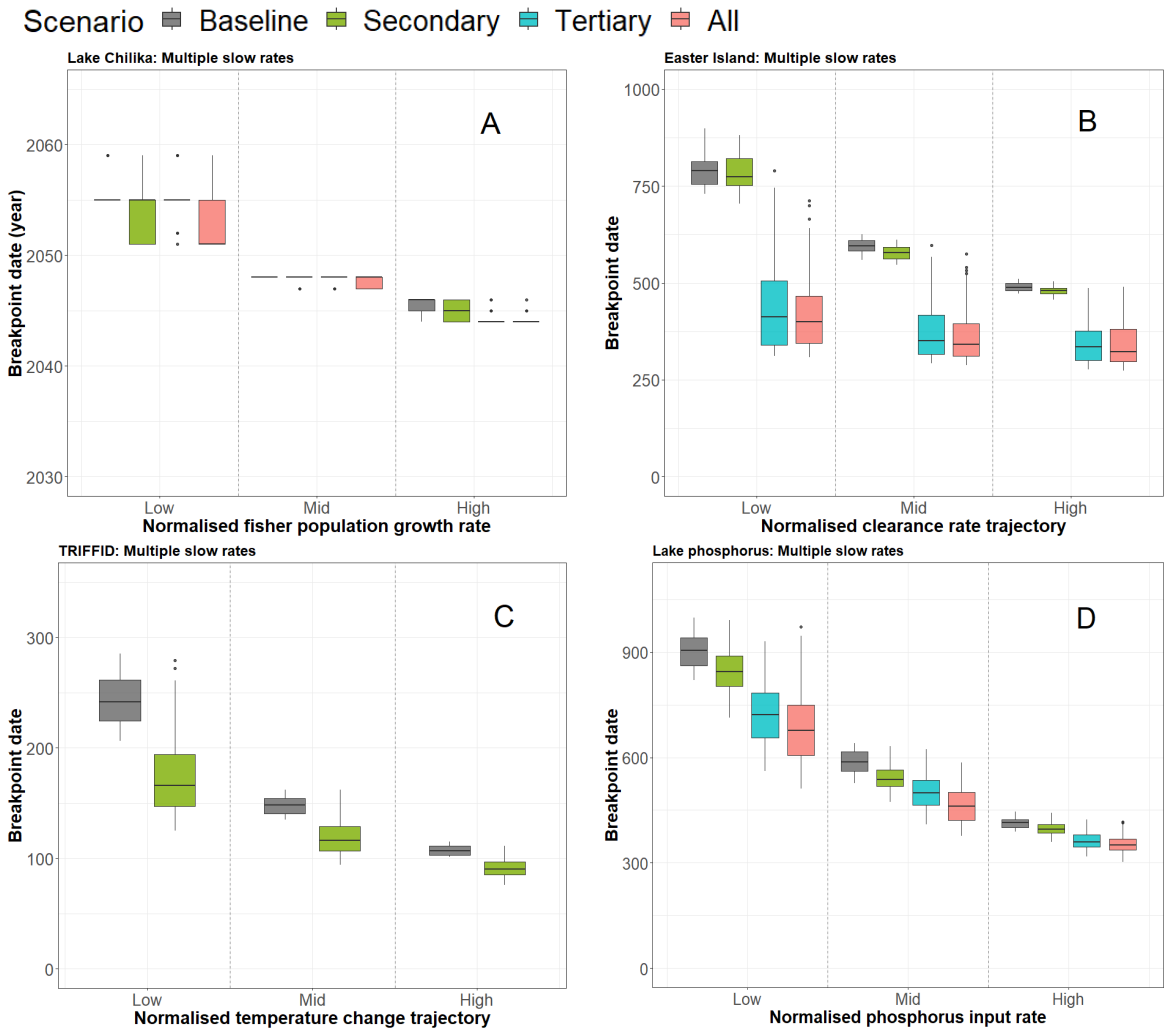

Figure S4-4: The relationship between the breakpoint date and the primary (baseline) slow driver (grey for the individual (grey) and multiple (coloured) drivers, when the breakpoint date is defined by the second alternative method described above (Type 2a boundaries). *As in the main manuscript (i.e., Figures 2-4), the normalised primary driver trajectories are apportioned into three discrete ranges: 'low' – 0.25-0.35, 'mid' – 0.45-0.55, and 'high' – 0.65-0.75. For comparison with the main manuscript, this figure is the equivalent of Figure 2. Subplots: (A) Lake Chilika model, primary slow driver: fisher population growth, secondary driver: climate change, tertiary driver: fish price; (B) Easter Island model, primary slow driver = tree clearance, secondary driver: agricultural carrying capacity, tertiary driver: tree mortality; (C) TRIFFID model, primary slow driver: temperature change, secondary driver: disturbance rate; (D) Lake phosphorus model, primary slow driver: phosphorus external input, secondary driver: phosphorus recycling rate, tertiary driver: phosphorus sedimentation rate. Breakpoint date units are the same as in Figure S2-1. Boxplot dimensions are as Figure 2. The number of simulations (n) underpinning each primary driver trajectory range (i.e., low, middle, and high) in each of the above subplots are as follows: (A) 185, 225, 200; (B) 317, 347 and 359; (C) 400, 402, 315; (D) 408, 402 and 315.*

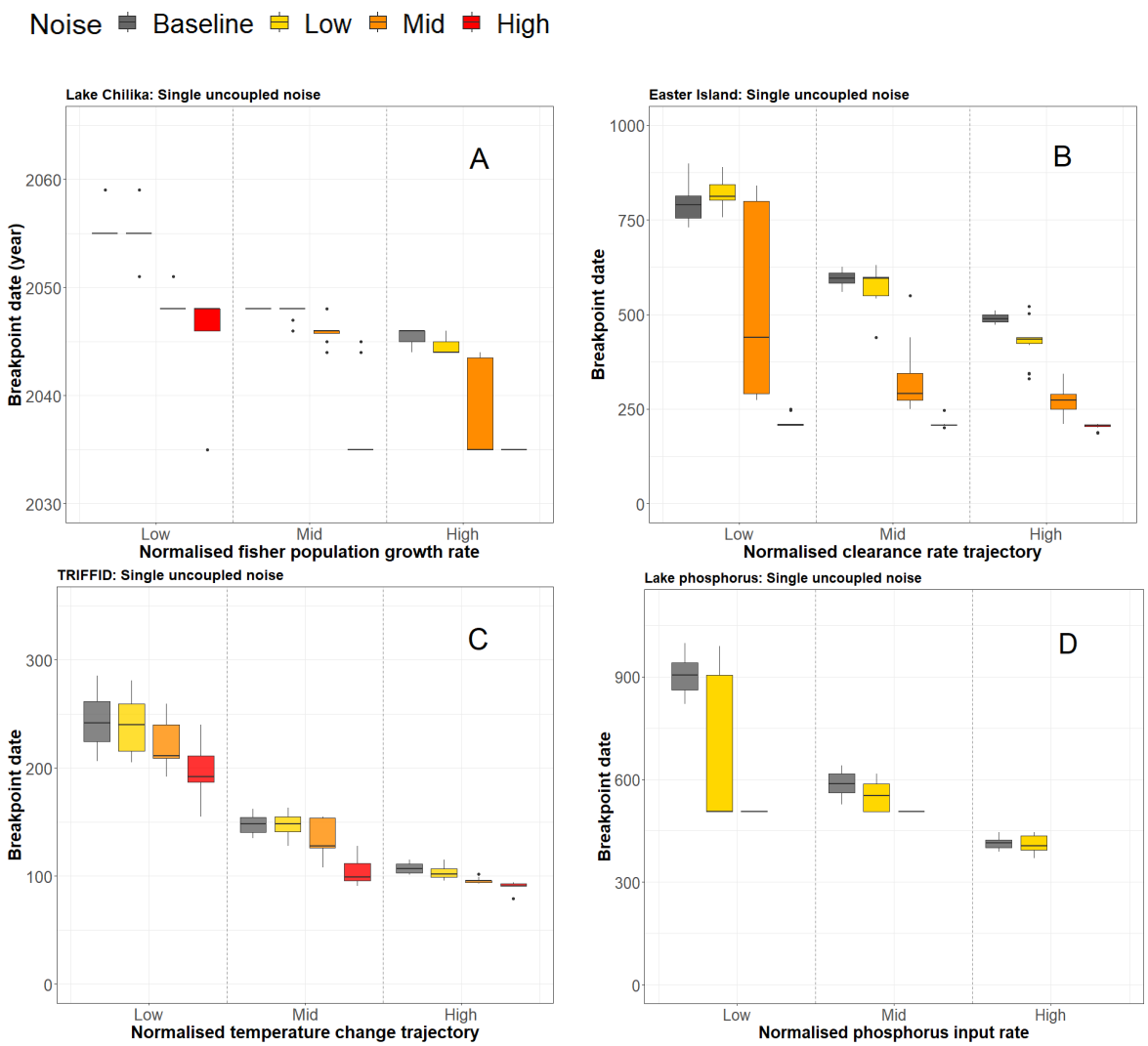

Figure S4-5: The relationship between the breakpoint date and the primary slow driver (grey) for varying levels of uncoupled noise in the primary slow driver (σ), where normalised σ values ≤ 0.333 signify 'low noise' (yellow), normalised σ values > 0.333 and ≤ 0.666 signify 'mid noise' (orange), and normalised σ values > 0.666 signify 'high noise' (red) (Methods Section 2.3). The breakpoint date is defined by the second alternative method described above (Type 2a boundaries). *As in the main manuscript (i.e., Figures 2-4), the normalised primary driver trajectories are apportioned into three discrete ranges: 'low' – 0.25-0.35, 'mid' – 0.45-0.55, and 'high' – 0.65-0.75. For comparison with the main manuscript, this figure is the equivalent of Figure 3. Subplots: (A) Lake Chilika model outputs, primary slow driver = fisher population growth; (B) Easter Island model outputs, primary slow driver = tree clearance; (C) TRIFFID model outputs, primary slow driver = temperature change; (D) Lake phosphorus model outputs, primary slow driver = phosphorus input. Model timestep units are the same as in Figure S2-1. Boxplot dimensions are as Figure 2. The number of simulations (n) underpinning each primary driver trajectory range (i.e., low, middle, and high) in each of the above subplots are as follows: (A) 78, 82 and 79; (B) 88, 120 and 140; (C) 409, 401 and 389; (D) 86, 135 and 140.*

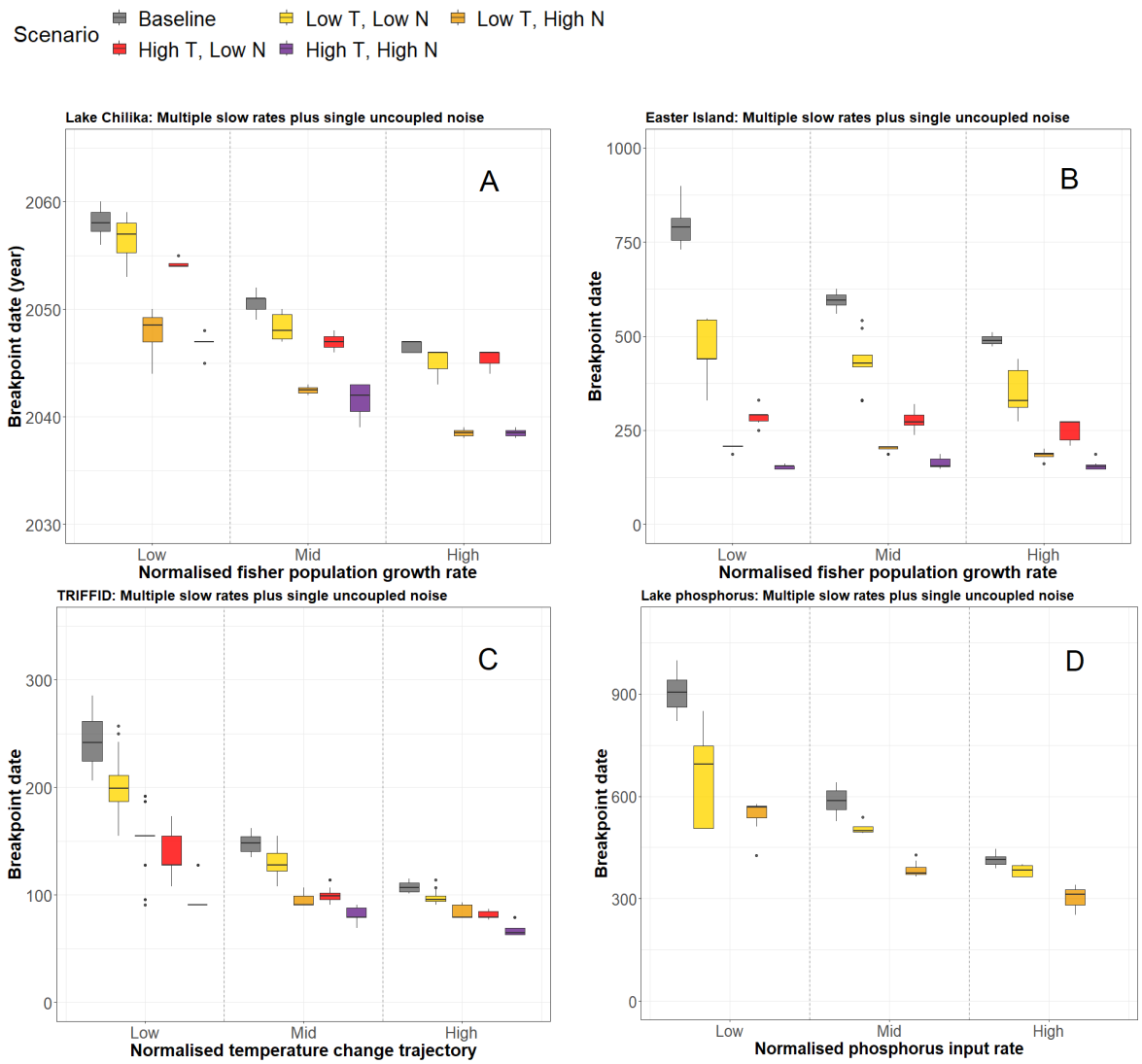

Figure S4-6: The relationship between the breakpoint date and the primary slow driver (grey) when weak (normalised T values ≤ 0.333) and strong (normalised T values > 0.666) multiple driver trajectories are combined with weak (normalised σ values ≤ 0.333) and strong (normalised σ values > 0.666) uncoupled noise (T = trajectory, N = noise). The breakpoint date is defined by the second alternative method described above (Type 2a boundaries). *As in the main manuscript (i.e., Figures 2-4), the normalised primary driver trajectories are apportioned into three discrete ranges: 'low' – 0.25-0.35, 'mid' – 0.45-0.55, and 'high' – 0.65-0.75. For comparison with the main manuscript, this figure is the equivalent of Figure 4. Subplots: (A) the Lake Chilika model, primary slow driver = fisher population growth, additional driver: climate change and fish price; (B) the Easter Island model, primary slow driver = tree clearance, additional drivers: agricultural carrying capacity and tree mortality; (C) the TRIFFID model, primary slow driver = temperature change, additional driver: disturbance rate; (D) the Lake phosphorus model, primary slow driver = phosphorus, additional drivers: phosphorus recycling rate, phosphorus sedimentation rate. Note, the first 10,000 simulations of the Lake phosphorus model (subplot D) did not produce any outcomes between the 0.25-0.35, 0.45-0.55 and 0.65-0.75 primary driver ranges within the 'high trajectory, high noise' scenario. Model timestep units are the same as in Figure S2-1. Boxplots dimensions are as Figure 2. The number of simulations (n) underpinning each primary driver trajectory range (i.e., low, middle, and high) in each of the above subplots are as follows: (A) 45, 60 and 43; (B) 82, 96 and 94; (C) 340, 330 and 315; (D) 75, 95 and 65.*

Implications

Although the average and variance in breakpoint dates differ quantitatively under the alternative boundary definitions (Table S4-1), the experiments conducted here provide confidence that the overarching findings and implications remain robust to the type of definition used to define the breakpoints. First, across all four models, we find that an increase in the baseline trajectory leads to earlier breakpoints under both of the alternative definitions (Figures S4-1 to S4-6). Second, the decrease in the breakpoint date with increasing baseline trajectories retains the form of a nonlinear decay across all four models and both boundary definitions, whereby the breakpoint date is most sensitive to a unit change in the primary driver at lower trajectory levels (Figures S4-1 to S4-6). Third, the addition of extra drivers continues to cause breakpoints to emerge at lower levels of the primary driver than under the baseline scenario alone (i.e., to the left of the dashed vertical line in Figures S4-7 to S4-12). Fourth, under both alternative boundary definitions, the earliest breakpoints occur under the combination of high baseline trajectories, active secondary and tertiary drivers, and relatively high system noise (Figures S4-3 and S4-6). Lastly, in terms of the single noise scenarios, the ramping up of noise leads to earlier breakpoints across all four models and both alternative definitions (Figures S4-2 and S4-5).

Table S4-1 highlights a key difference between the boundary definitions. Amongst the first 10,000 simulations, the original 'abrupt type-3 threshold' identifies fewer breakpoints than the type 1a and type 2a methods. This is because in order to confidently date the breakpoint, the method [9] based on identifying when regression coefficients shift from one stable regime to another requires sufficient timesteps after the potential breakpoint to ascertain whether the shift was significant. As a consequence, a potential abrupt type-3 threshold occurring close to the end of a simulation does not have sufficient timesteps downstream for the model of Zeileis *et al.*[9] to date the switch in regression coefficients with an adequate degree of confidence. In contrast, the two alternative boundary methods are not reliant on such significance tests, meaning the last timestep can be captured if it is the steepest change in the outcome over time or the first with an outcome value below 20% of the original. As a consequence, across all four models (Table S4-1), the maximum breakpoint dates under the type 1a and type 2a boundaries occur consistently later than under the type 3a definition.

Table S4-1: Descriptive comparison of the number, average and distribution of breakpoints under the original ('abrupt type-3 threshold') and alternative breakpoint definitions across the first 10,000 simulations in each of the four models. Note the statistics for the first 10,000 simulations below do not distinguish between the four different scenario types (i.e., Baseline, Multi-driver [e.g., Figure 2], uncoupled noise [e.g., Figure 3] and uncoupled noise plus multi-drivers [e.g., Figure 4]). BP = breakpoint.

Model	Boundary definition	No. BP	Median BP date	Mean BP date	BP date standard deviation	Maximum BP date	Minimum BP date
Lake Chilika	Original	5287	2042	2043.4	8.45	2077	2028
	Type 1a	9768	2047	2050.3	11.1	2100	2036
	Type 2a	9768	2046	2045.8	9.45	2081	2035
Easter Island	Original	4974	574	618.4	245.7	1273	225
	Type 1a	8927	346	403.9	218.2	1496	164
	Type 2a	8927	295	359.1	205.7	1462	12
TRIFFID	Original	7778	116	146.6	80.7	424	75
	Type 1a	9283	110	147.2	89.8	500	45
	Type 2a	9283	108	143.9	87.0	500	42
Lake phosphorus	Original	4547	434	473.8	150.9	849	249
	Type 1a	7307	362	388.6	225.0	999	27
	Type 2a	4555	457	488.8	182.9	999	152

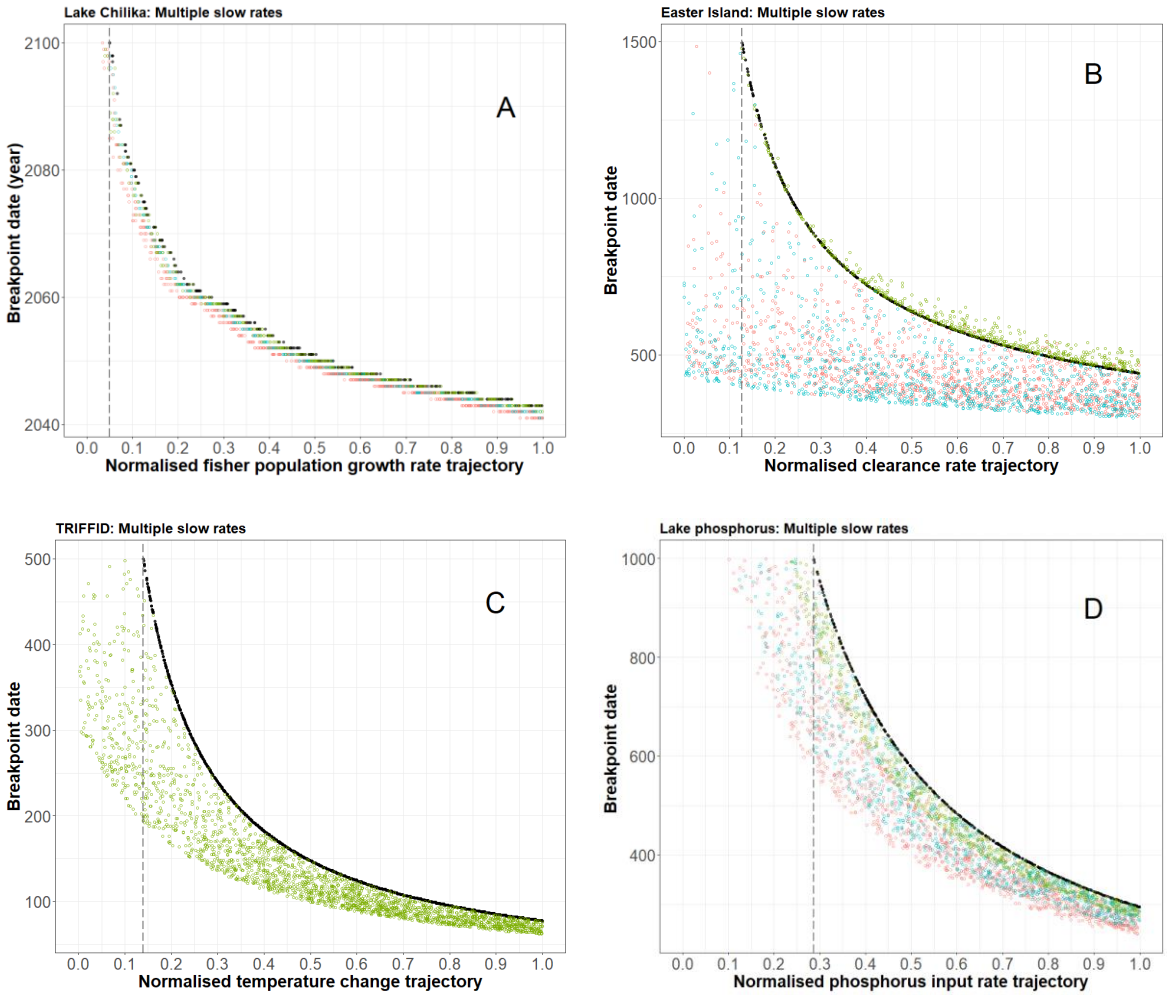

Figure S4-7: Scatter plots depicting the raw data producing the boxplots in Figure S4-1. *The dashed grey vertical line represents the weakest primary driver value associated with an ATDC in each plot. Subplots: (A) Lake Chilika model outputs, primary slow driver: fisher population growth; (B) Easter Island model outputs, primary slow driver = tree clearance; (C) TRIFFID model outputs, primary slow driver = temperature change; (D) Lake phosphorus model outputs, primary slow driver = phosphorus input. Model timestep units are the same as in Figure S2-1.*

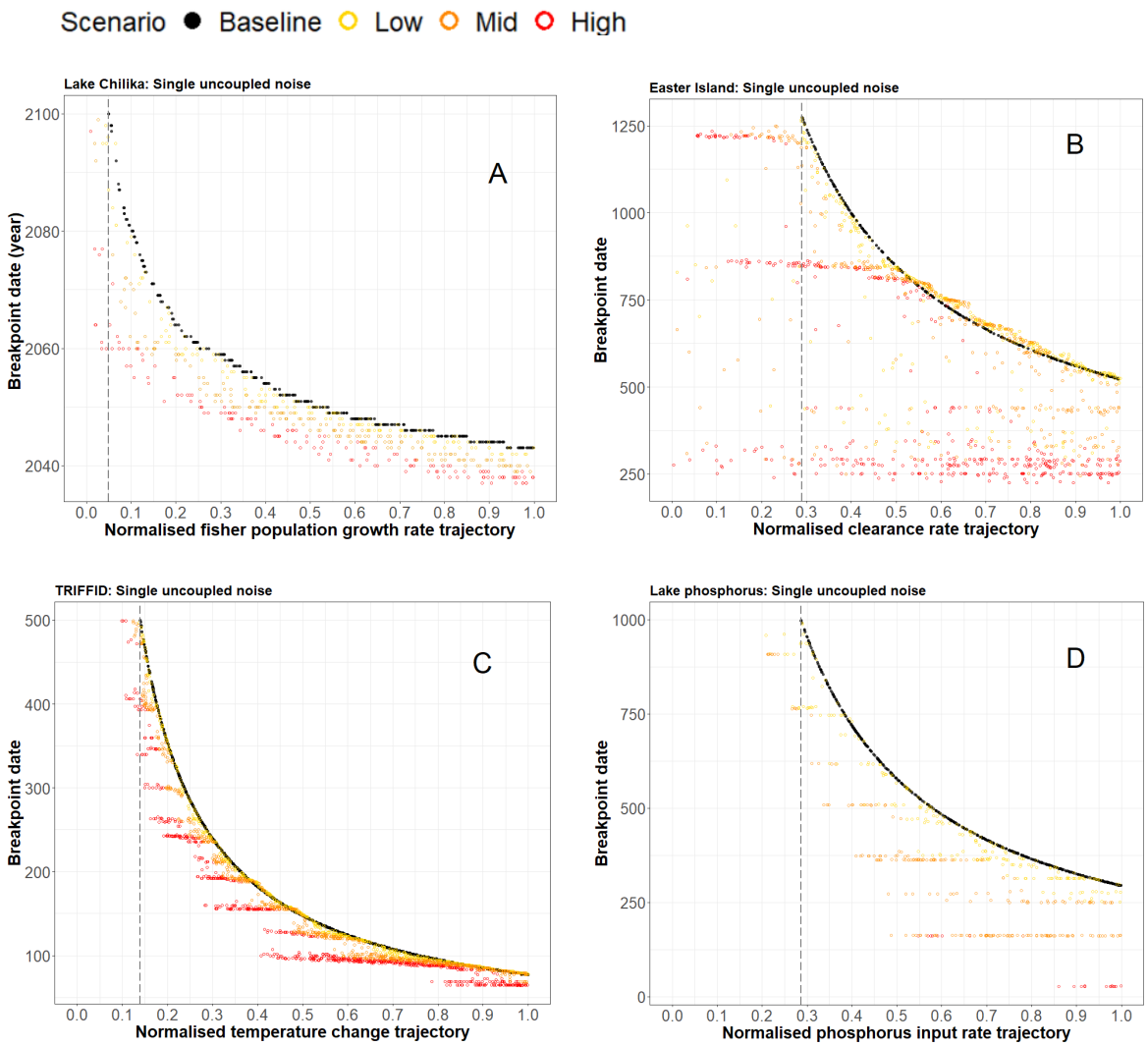

Figure S4-8: Scatter plots depicting the raw data producing the boxplots in Figure S4-2. *The dashed grey vertical line represents the weakest primary driver value associated with an ATDC in each plot. Subplots: (A) Lake Chilika model outputs, primary slow driver: fisher population growth; (B) Easter Island model outputs, primary slow driver = tree clearance; (C) TRIFFID model outputs, primary slow driver = temperature change; (D) Lake phosphorus model outputs, primary slow driver = phosphorus input. Model timestep units are the same as in Figure S2-1.*

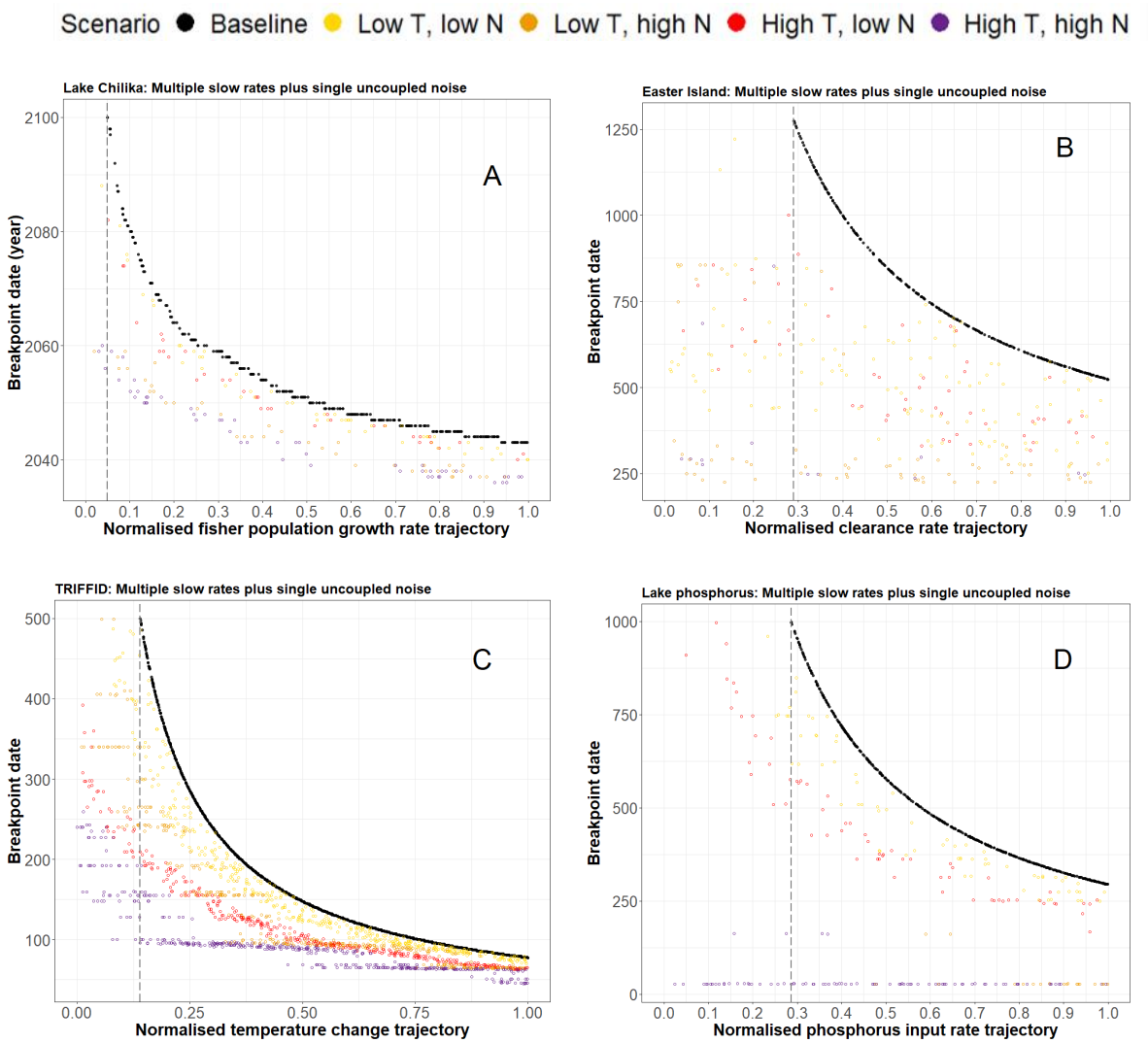

Figure S4-9: Scatter plots depicting the raw data producing the boxplots in Figure S4-3. *The dashed grey vertical line represents the weakest primary driver value associated with an ATDC in each plot. Subplots: (A) Lake Chilika model outputs, primary slow driver: fisher population growth; (B) Easter Island model outputs, primary slow driver = tree clearance; (C) TRIFFID model outputs, primary slow driver = temperature change; (D) Lake phosphorus model outputs, primary slow driver = phosphorus input. Model timestep units are the same as in Figure S2-1.*

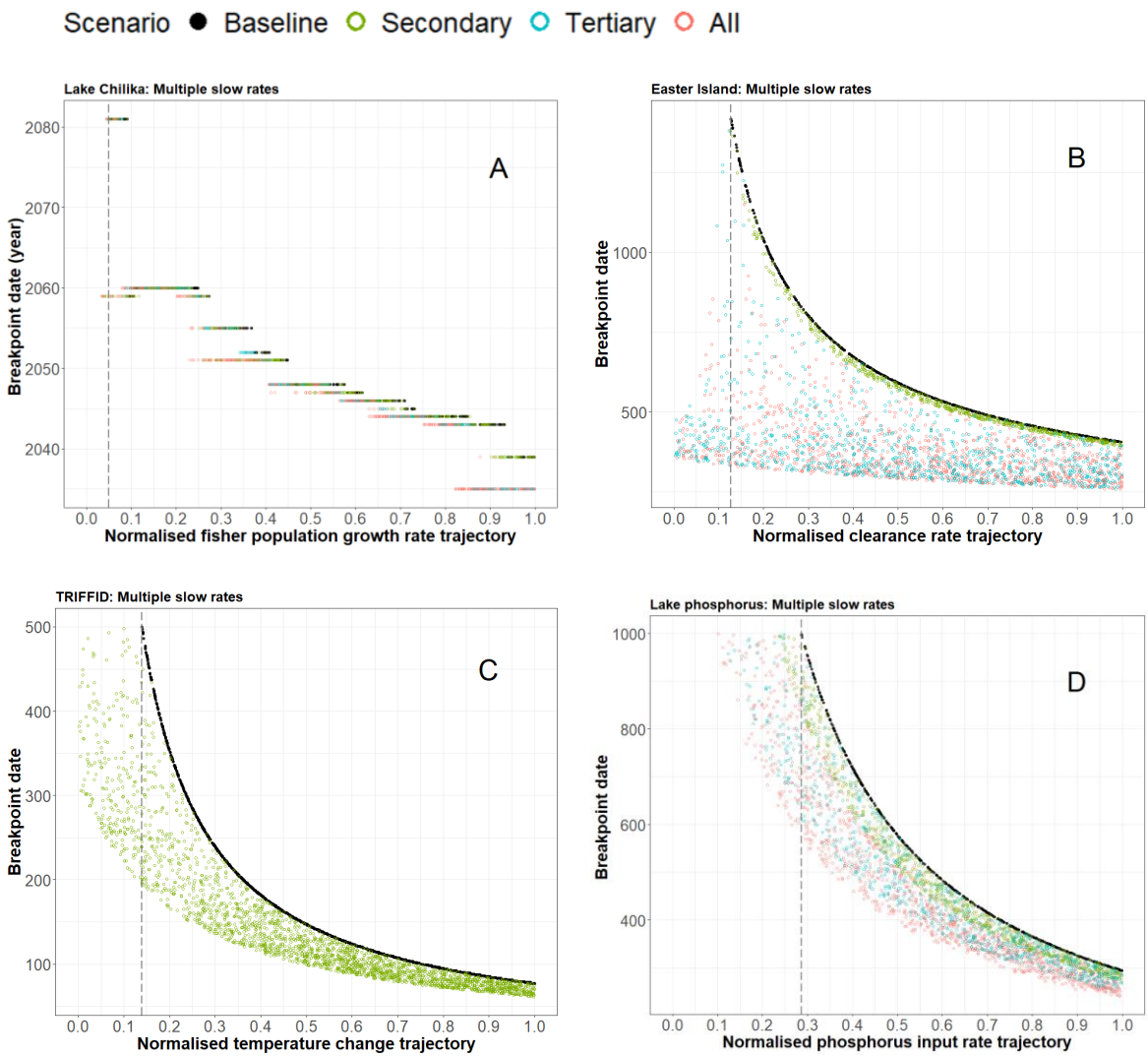

Figure S4-10: Scatter plots depicting the raw data producing the boxplots in Figure S4-4. *The dashed grey vertical line represents the weakest primary driver value associated with an ATDC in each plot. Subplots: (A) Lake Chilika model outputs, primary slow driver: fisher population growth; (B) Easter Island model outputs, primary slow driver = tree clearance; (C) TRIFFID model outputs, primary slow driver = temperature change; (D) Lake phosphorus model outputs, primary slow driver = phosphorus input. Model timestep units are the same as in Figure S2-1.*

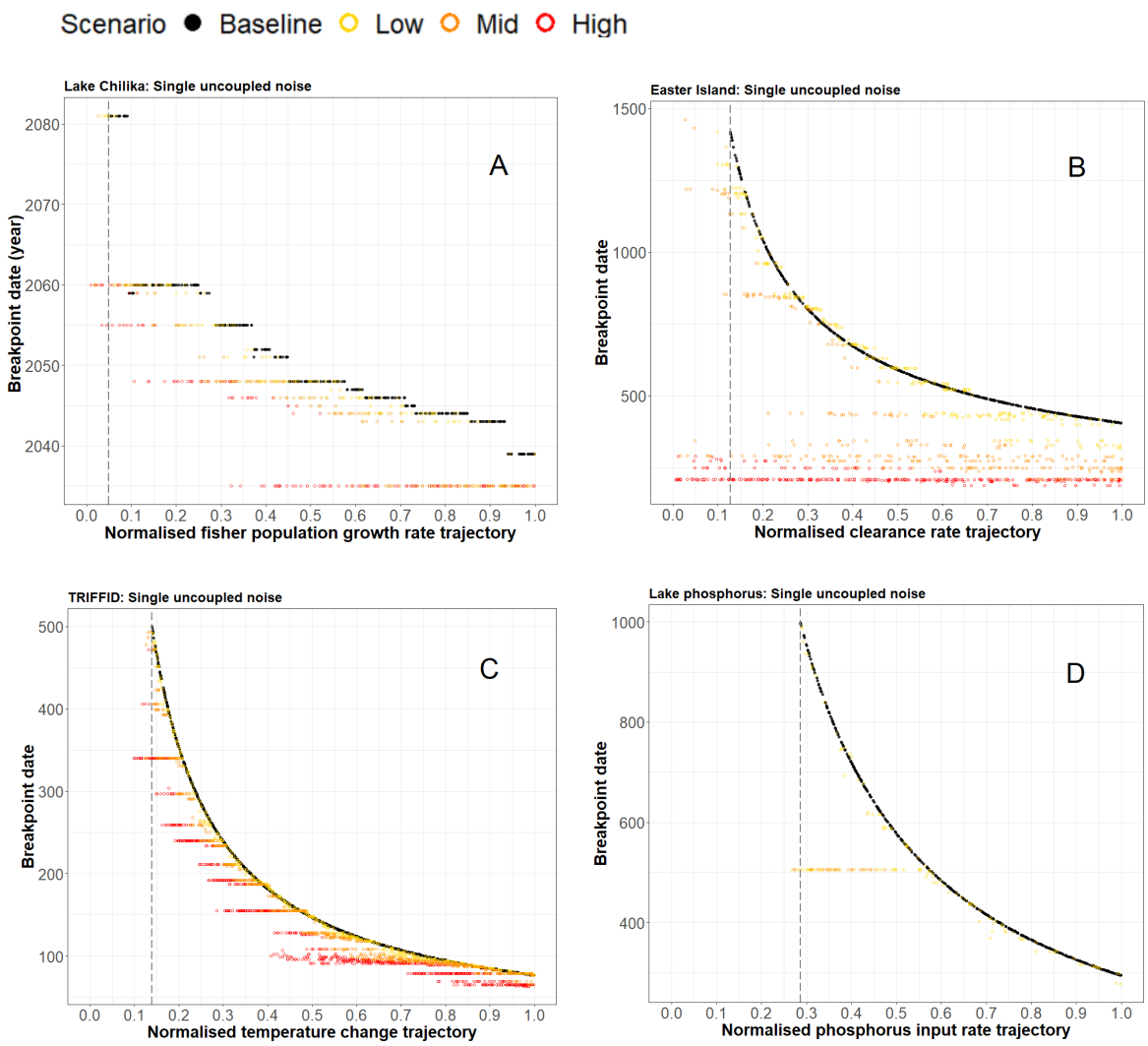

Figure S4-11: Scatter plots depicting the raw data producing the boxplots in Figure S4-5. *The dashed grey vertical line represents the weakest primary driver value associated with an ATDC in each plot. Subplots: (A) Lake Chilika model outputs, primary slow driver: fisher population growth; (B) Easter Island model outputs, primary slow driver = tree clearance; (C) TRIFFID model outputs, primary slow driver = temperature change; (D) Lake phosphorus model outputs, primary slow driver = phosphorus input. Model timestep units are the same as in Figure S2-1.*

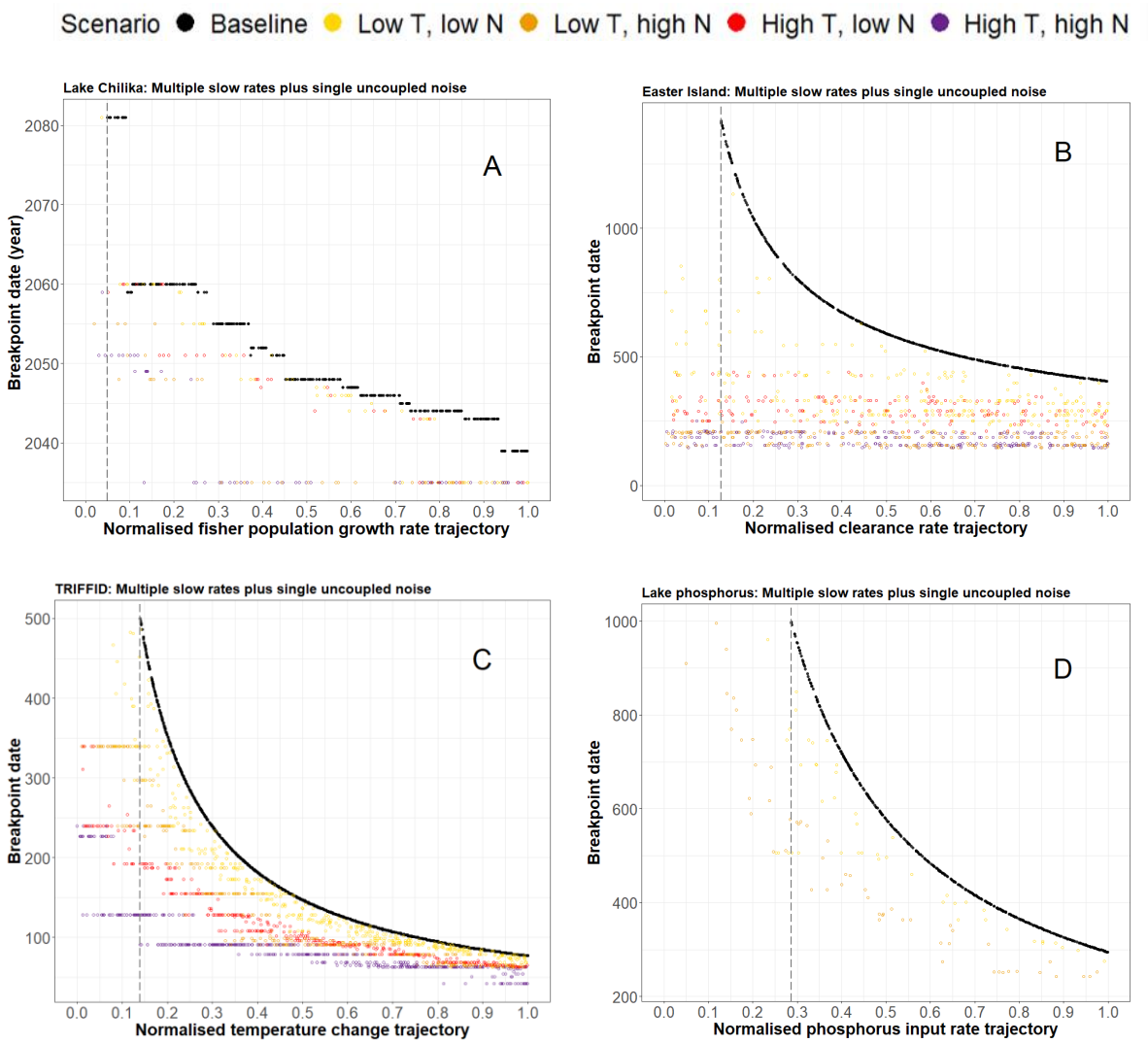

Figure S4-12: Scatter plots depicting the raw data producing the boxplots in Figure S4-6. *The dashed grey vertical line represents the weakest primary driver value associated with an ATDC in each plot. Subplots: (A) Lake Chilika model outputs, primary slow driver: fisher population growth; (B) Easter Island model outputs, primary slow driver = tree clearance; (C) TRIFFID model outputs, primary slow driver = temperature change; (D) Lake phosphorus model outputs, primary slow driver = phosphorus input. Model timestep units are the same as in Figure S2-1.*

SI-5: Cumulative Stress Versus Breakpoint Date

Introduction and methods

Systems vary in their sensitivity to driver rates and amounts of cumulative stress [e.g. Matthews *et al.*[13]]. Simple systems may reach a critical threshold when a specific condition or stress level is reached independent of driver rate. More complex, resilient systems will show different responses to stress levels depending on the loss of resilience caused by an inability of balancing feedback mechanisms to absorb stress as driver rates increase. We explore the importance of driver rate and cumulative stress in the breakpoint patterns observed in Figures 2 to 4 of the main manuscript. As stated in the Introduction, we hypothesised that an increase in the number of drivers will bring forward the timing of breakpoints in systems already under stress from slow drivers; as such, what are the implications of adding extra stresses for the overall level of stress a system can absorb before undergoing an ATDC?

We explore these questions by mapping the breakpoint dates of the first 5,000 multi-driver simulations in each model (Figure 2, main manuscript) against the total cumulative stress that accumulates in each simulation until the breakpoint. The total cumulative stress measure is a simple cumulative sum of the normalised primary, secondary and tertiary driver values at each timestep up until and including the breakpoint date (as calculated by the approach detailed in Methods Section 3.2). See an illustrative example of this calculation below, for a simulation that would be considered an 'All' scenario in Figure 2 of the main manuscript (note, the breakpoint date has been set artificially low in order to illustrate the general methodology):

$$Breakpoint\ date_i = 4$$

$$Normalised\ primary\ driver\ values_{i,t} = 0, 0.1, 0.2, 0.3$$

$$Normalised\ secondary\ driver\ values_{i,t} = 0, 0.05, 0.1, 0.15$$

$$Normalised\ tertiary\ driver\ values_{i,t} = 0, 0.04, 0.08, 0.12$$

$$Cumulative\ primary\ stress\ at\ breakpoint_{i,t=4} = 0.6$$

$$Cumulative\ secondary\ stress\ at\ breakpoint_{i,t=4} = 0.3$$

$$Cumulative\ primary\ stress\ at\ breakpoint_{i,t=4} = 0.24$$

$$Total\ cumulative\ stress\ at\ breakpoint_{i,t=4} = 0.6 + 0.3 + 0.24 = 1.14$$

Where i is the simulation number (i.e., 1, 2… 5000) and t is the timestep.

Results

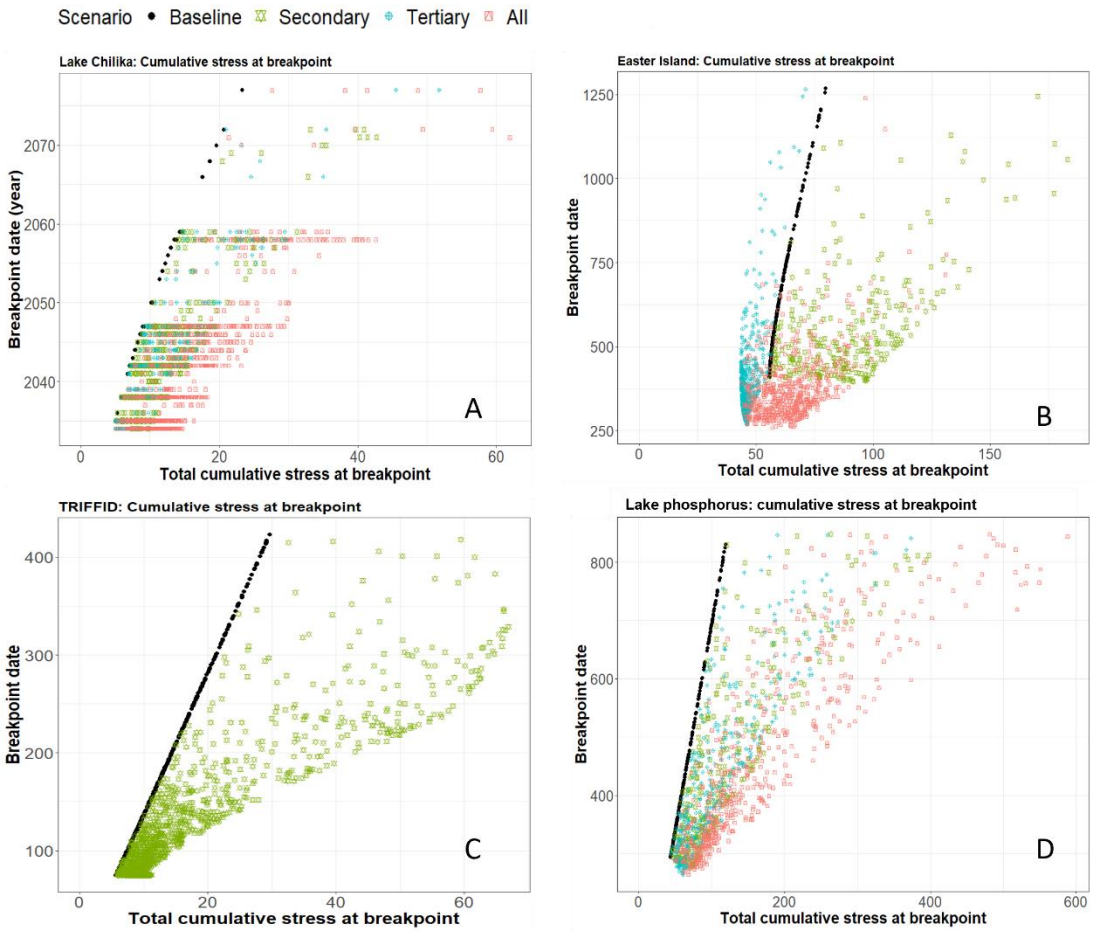

Figure S5-1: The relationship between the breakpoint date and the total cumulative stress up until the breakpoint for the individual (black) and multiple (coloured) drivers. *Subplots: (A) Lake Chilika model, primary slow driver: fisher population growth, secondary driver: climate change, tertiary driver: fish price; (B) Easter Island model, primary slow driver = tree clearance, secondary driver: agricultural carrying capacity, tertiary driver: tree mortality; (C) TRIFFID model, primary slow driver: temperature change, secondary driver: disturbance rate; (D) Lake phosphorus model, primary slow driver: phosphorus external input, secondary driver: phosphorus recycling rate, tertiary driver: phosphorus sedimentation rate.*

Implications

The overall distribution of points in each panel shows that the breakpoint date is negatively related to cumulative stress with the most significant reductions in breakpoint date associated with the smallest amounts of cumulative stress. This does not support the idea that the stability of these systems is a simple function of cumulative stress. The fan shaped patterns illustrate that the amount of tolerated cumulative stress is related to driver rate: low driver rates (small reductions in breakpoint dates towards the top of each panel) are associated with wide ranges of cumulative stress, whereas high driver rates (large reductions in breakpoint date) are associated with small ranges of cumulative stress. At low driver rates, feedback mechanisms are able to absorb the stresses from additional drivers proportionately more effectively than at high rates. Nevertheless, for a given level of cumulative stress, the presence of additional drivers tends to produce earlier breakpoint dates (variation along the y-axis). This implies that while additional drivers obviously produce more stress, the first order control on breakpoint date is the main primary driver rate that controls system resilience. For example, for Lake Chilika (Figure S5-1A), a total cumulative stress of 18-22 with only the primary driver produces an average breakpoint date of 2069; in turn, the average breakpoint dates for the same total

cumulative stress range but under the Secondary, Tertiary and All scenarios equal 2054, 2053 and 2047, respectively.

The slight exception is for the Easter Island model which shows that the contribution of stress from the tertiary driver reduces the cumulative stress associated with breakpoint date driven by the primary driver alone (Figure S5-1B). For example, between the breakpoint date range of 490-510 (Figure S5-1B), the average total cumulative stress under the Baseline scenario is 56.8, whilst the equivalent figure is 48.2 for the Tertiary scenario (equivalent total cumulative stresses for Secondary and All are 87.6 and 72.9, respectively). This suggests that the rate of tree mortality has an equivalent or even larger impact on system resilience than the primary driver of temperature change.

Our results show that systems do not collapse at a constant level of cumulative stress irrespective of the rate (SI-5) but rather underline the importance of driver rates[14–16].

SI-6: Feedback Analysis – Loops That Matter

Introduction and methods

System dynamics models (SDM) are particularly adept at modelling ecosystems underpinned by feedback loop structures[17,18]. Akin to a home thermometer system, balancing or negative feedback loops are known to stabilise system dynamics, producing what is termed 'goal-seeking behaviour' over time. In contrast, as conceptualised by a snowball growing in mass as it runs downhill (the so-called "snowball effect"), reinforcing or positive feedback loops can produce runaway behaviours if left unabated. Critically for the approach taken below, balancing feedback loops are often given a nominal 'polarity score' of -1, whilst reinforcing feedback loops are given a polarity score of +1.

To further explain the distribution of breakpoint dates presented in Figures 2 to 4, we utilise the 'Loops That Matter' function (built-in to the SDM software STELLA[19]) to track the growth and decline of the key feedback loops driving system behaviours in each of the four models. In essence, the Loops That Matter (LTM) function describes the *relative* contribution of each feedback loop to model behaviour [full mathematical details of the approach are detailed in Schoenberg *et al.*[20]]. The LTM score for an individual feedback loop is calculated by multiplying together its constituent 'link scores' (i.e., connections between pairs of model variables), whereby a positive link score means that a change in the source (i.e., upstream) variable will cause the target variable (i.e., downstream) to change in the same direction, while a negative value means that a change in the source variable will cause the target variable to change in the opposite direction. Therefore, LTM scores for individual feedback loops can range between -100% and +100%, where the former would signify that a balancing feedback loop is responsible for 100% of model behaviour, and the latter would indicate that a reinforcing feedback loop is responsible for 100% of model behaviour. In the graphs below, the 'net feedback loop strength' is equal to the sum of the individual feedback scores at model each timestep.

We explore how the feedback loops in each of the models strengthen and weaken across two experiments (see Table S6-1 for a description of the key feedback loops in each model):

<u>LTM Experiment #1: Varying the baseline driver trajectory</u>

Across 5000 simulations per model, we explore how the feedback loops evolve in response to an increase in the baseline driver trajectories (with secondary and tertiary drivers remaining switched-off), as per the scenario funnels in Figure S2-2 (expressed numerically in Table S3-2). As per the x-axis bounds used to depict the boxplots in Figures 2 to 4, we visualise the simulations with normalised primary driver trajectories between 0.25-0.35, 0.45-0.55, and 0.65-0.75. The expectation here is that ramping up the growth rate of the baseline driver (i.e., steeper trajectories) will cause earlier collapses, which in turn will be associated with earlier growth in the relative importance of feedback loop(s) responsible for triggering instability in the system (e.g., reinforcing feedback loops).

<u>LTM Experiment #2: Increasing the number of drivers</u>

Across a separate set of 5000 simulations per model, we also investigate how adding secondary and tertiary drivers to the baseline influences the evolution of feedback loops underpinning system behaviour. In order to clearly visualise the timeseries dynamics and ensure that simulations are being compared across a consistent set of parameter value, we opt to constrain all driver trajectories between normalised values of 0.45 to 0.55, with secondary and tertiary drivers randomly switching on and off as per the Monte Carlo approach described in Methods Section 2. Consistent with the scenarios depicted in Figure 2, this approach produces 'Baseline', 'Secondary', 'Tertiary' and 'All' scenarios. It is expected that the addition of extra drivers will trigger the growth of reinforcing feedback loops earlier, which will then be associated with earlier abrupt changes in system outcomes.

Table S6-1: The key feedbacks influencing outcome behaviours in each of the four models.
Key feedbacks are defined by STELLA as those which combine to explain at least 80% of total model behaviour over the respective model horizons (e.g., TRIFFID = 500 timesteps). Feedbacks denoted below with the prefix 'R' are reinforcing, whilst feedbacks with the prefix 'B' are balancing.

Model	Feedback	Description
Lake Chilika[18,21]	R1	*Growth in the traditional fisher population:* For a given fisher population growth rate ('r') and livelihood carrying capacity, the number of new traditional fishers entering the lagoon at any given timestep is proportional to their population.
	R2	*Growth in the motorised fisher population:* For a given fisher population growth rate ('r') and livelihood carrying capacity, the number of new fishers using motorboats who enter the lagoon at any given timestep is proportional to their population.
	B1	*Traditional fleet catch limitation:* The number of fish the traditional fisher fleet can catch for a given level of effort is proportional to the fish population density; as the fish density declines, so too does the efficiency of the traditional fishing effort.
	B2	*Motorboat fleet catch limitation:* The number of fish the motorboat fisher fleet can catch for a given level of effort is proportional to the fish population density; as the fish density declines, so too does the efficiency of the motorboat fishing effort.
Easter Island[22]	B1	*Rat population growth:* As a form of ecological carrying capacity, the rat population growth rate declines as the number of rats on the island increase.
	B2	*Human population growth:* As a form of social-ecological carrying capacity, the human population growth rate declines as tree clearance intensifies.
	B3	*Rat-dependent tree population growth:* As the tree population grows, so too does the population of rats, which then limits the tree population in future.
	B4	*Clearance-dependent tree population growth:* As the tree population grows, so too does the clearance rate, which causes the tree population growth rate to decline.
TRIFFID[23,24]	R1	*Collapse in vegetation coverage:* The vegetation growth rate slows as the temperature increases above the optimal temperature for vegetation. Lower vegetation coverage increases the surface temperature, which further reduces the vegetation growth rate.
	B1	*Ecological carrying capacity:* Vegetation growth slows as vegetation fraction in the model increases.
Lake phosphorus[25,26]	R1	*Lake water phosphorus accumulation:* Reinforcing feedback between lake water phosphorus concentration and phosphorus recycling back into the water from the sediment.

Results

LTM Experiment #1: Varying the baseline driver trajectory

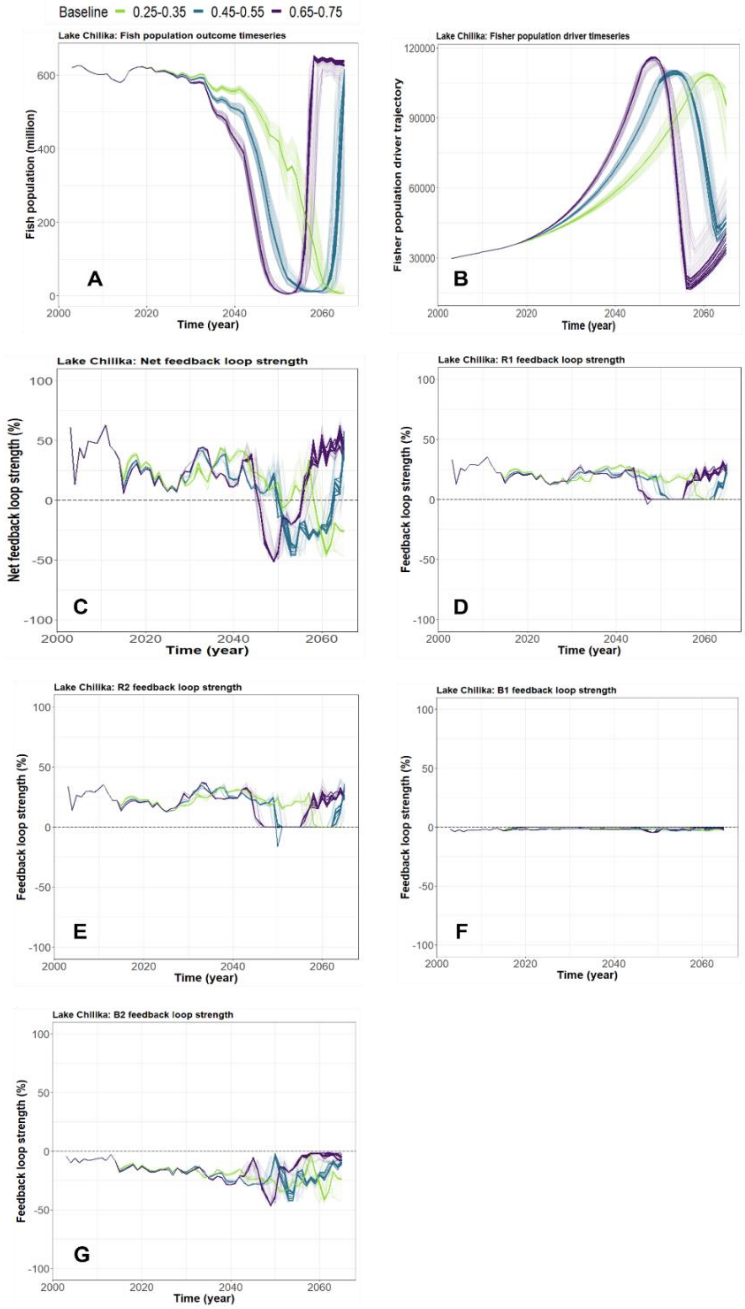

Figure S6-1: Timeseries outcomes from the first LTM experiment (Lake Chilika model), where the baseline driver strength was increased over three trajectory ranges. *See Table S6-1 for descriptions of the two reinforcing (subplots D-E) and two balancing feedbacks (subplots F-G) responsible for driving the dynamics of the fish population (subplot A) over time. Subplots: (A) Timeseries of the modelled Lake Chilika fish population; (B) Timeseries of the primary driver (fisher population); (C) Timeseries of the net feedback loop strength (i.e., reinforcing minus balancing strengths); (D) Timeseries of percentage contribution of feedback R1 to model behaviour; (E) Timeseries of percentage contribution of feedback R2 to model behaviour; (F) Timeseries of percentage contribution of feedback B1 to model behaviour; (G) Timeseries of percentage contribution of feedback B2 to model behaviour. Simulations that are within ±0.5% of the median primary driver trajectory are given a transparency value of 1 (i.e., opaque), while all other simulations are given a transparency (alpha value) of 0.05 in the R package 'ggplot'.*

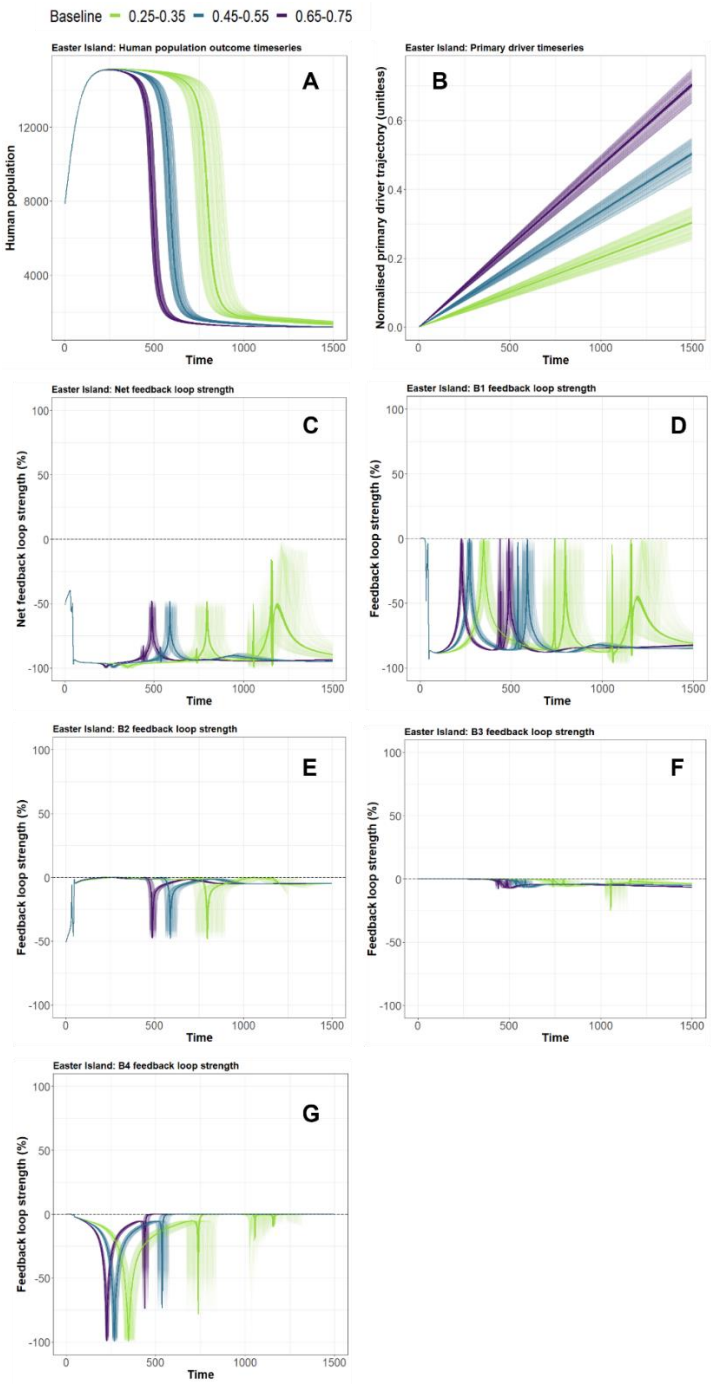

Figure S6-2: Timeseries outcomes from the first LTM experiment (Easter Island), where the baseline driver strength was increased over three trajectory ranges. *See Table S6-1 for descriptions of the four balancing feedbacks (subplots D-G) responsible for driving the dynamics of the human population (subplot A) over time. Subplots: (A) Timeseries of the modelled Easter Island human population; (B) Timeseries of the normalised primary driver magnitude; (C) Timeseries of the net feedback loop strength (i.e., reinforcing minus balancing strengths); (D) Timeseries of percentage contribution of feedback B1 to model behaviour; (E) Timeseries of percentage contribution of feedback B2 to model behaviour; (F) Timeseries of percentage contribution of feedback B3 to model behaviour; (G) Timeseries of percentage contribution of feedback B4 to model behaviour. As per Figure S6-1, simulations within ±0.5% of the median primary driver trajectory are given a transparency value of 1 (i.e., opaque), while all other simulations are given a transparency (alpha value) of 0.05 in the R package 'ggplot'.*

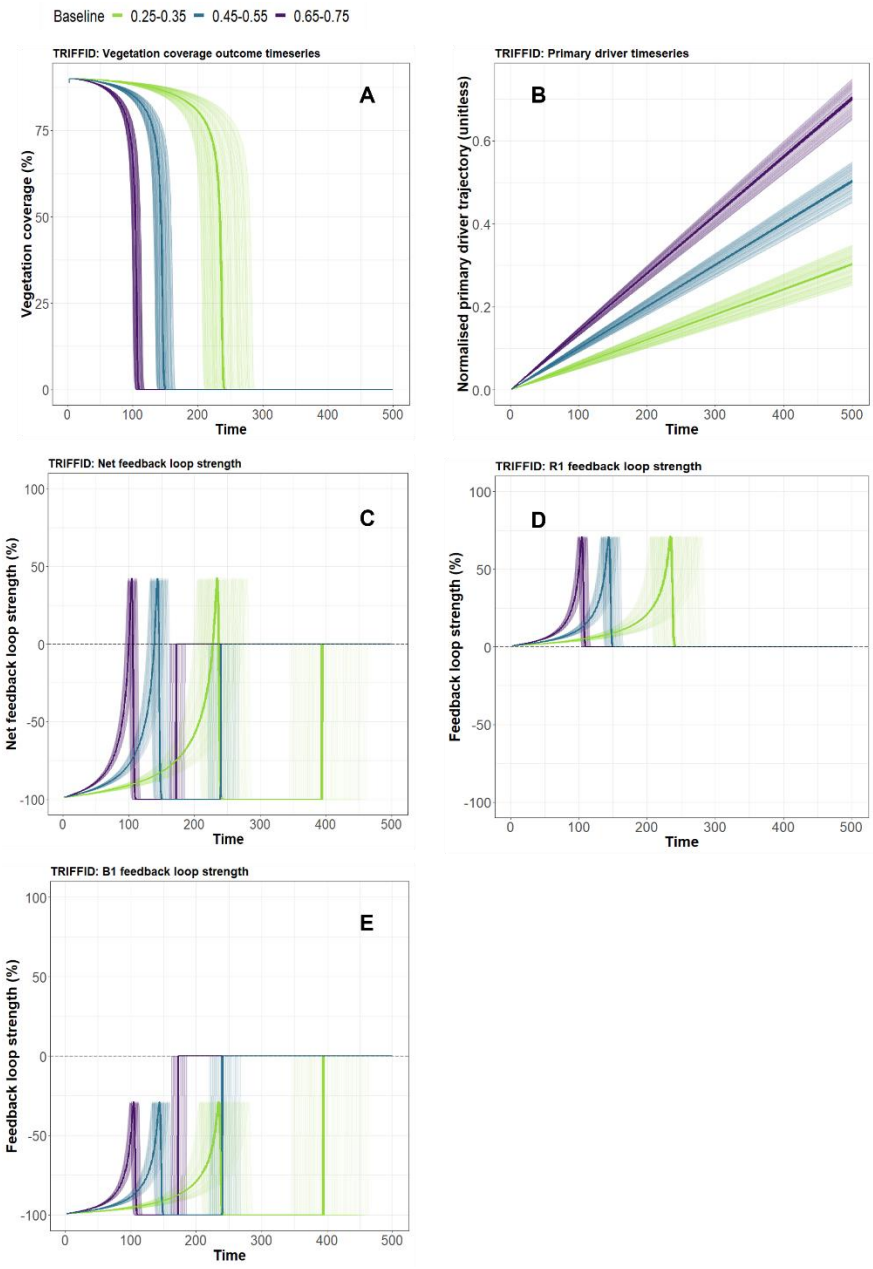

Figure S6-3: Timeseries outcomes from the first LTM experiment (TRIFFID), where the baseline driver strength was increased over three trajectory ranges. *See Table S6-1 for descriptions of the one reinforcing (subplot D) and one balancing feedback (subplots E) responsible for driving the dynamics of the tree coverage outcome (panel A) over time. Subplots: (A) Timeseries of the modelled vegetation coverage; (B) Timeseries of the normalised primary driver magnitude; (C) Timeseries of the net feedback loop strength (i.e., reinforcing minus balancing strengths); (D) Timeseries of percentage contribution of feedback R1 to model behaviour; (E) Timeseries of percentage contribution of feedback B1 to model behaviour. As per Figure S6-1, simulations within ±0.5% of the median primary driver trajectory are given a transparency value of 1 (i.e., opaque), while all other simulations are given a transparency (alpha value) of 0.05 in the R package 'ggplot'.*

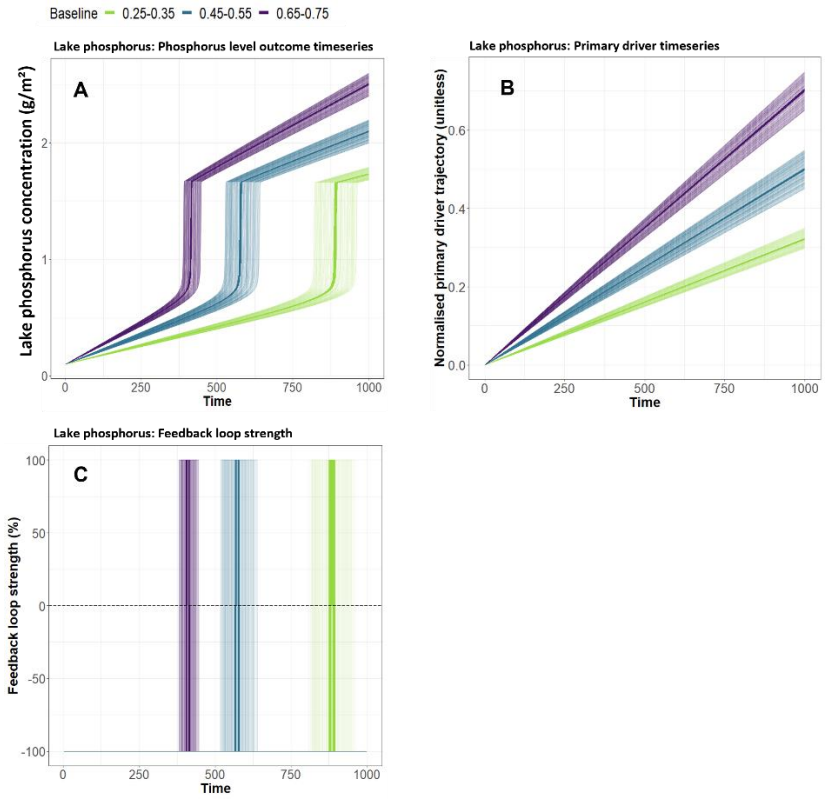

Figure S6-4: Timeseries outcomes from the first LTM experiment (Lake phosphorus), where the baseline driver strength was increased over three trajectory ranges. *See Table S6-1 for descriptions of the reinforcing feedback (C) responsible for driving the dynamics of the lake water phosphorus concentration (A) over time. Note that subplot C also acts as the net feedback strength, given that there is only one feedback in the Lake phosphorus model. Subplots: (A) Timeseries of the modelled lake phosphorus levels; (B) Timeseries of the normalised primary driver magnitude; (C) Timeseries of the percentage contribution of the single feedback loop to the model behaviour. As per Figure S6-1, simulations within ±0.5% of the median primary driver trajectory are given a transparency value of 1 (i.e., opaque), while all other simulations are given a transparency (alpha value) of 0.05 in the R package 'ggplot'.*

LTM Experiment #2: Increasing the number of drivers

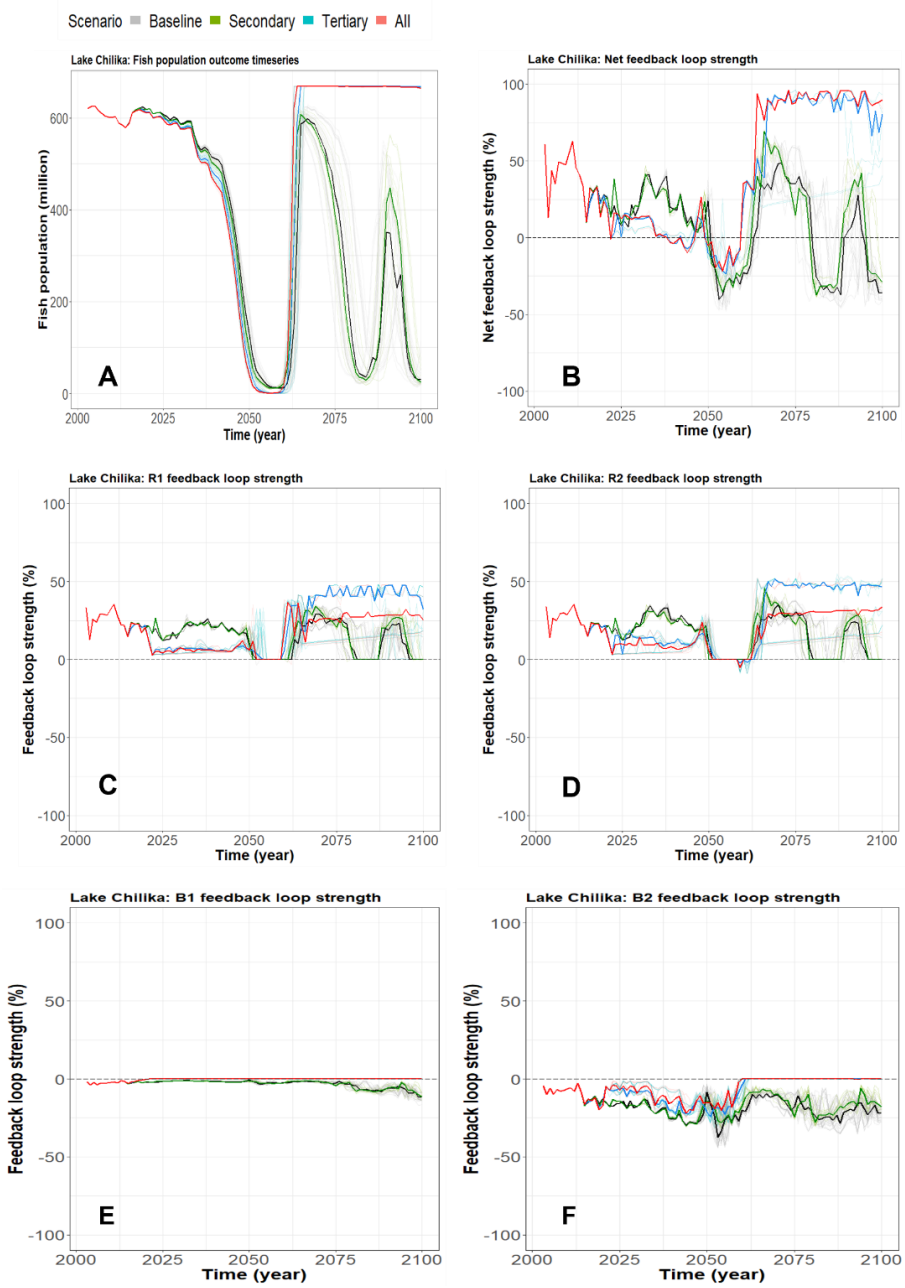

Figure S6-5: Timeseries outcomes from the second LTM experiment (Lake Chilika model) which held the baseline driver trajectory constant but added secondary and tertiary trajectories. *See Table S6-1 for descriptions of the two reinforcing and two balancing feedbacks (subplot C-F) responsible for driving the dynamics of the fish population (subplot A) over time. Subplots: (A) Timeseries of the modelled Lake Chilika fish population; (B) Timeseries of the net feedback loop strength (i.e., reinforcing minus balancing strengths); (C) Timeseries of percentage contribution of feedback R1 to model behaviour; (D) Timeseries of percentage contribution of feedback R2 to model behaviour; (E) Timeseries of percentage contribution of feedback B1 to model behaviour; (F) Timeseries of percentage contribution of feedback B2 to model behaviour. As per Figure S6-1, simulations within ±0.5% of the median primary driver trajectory are given a transparency value of 1 (i.e., opaque), while all other simulations are given a transparency (alpha value) of 0.05 in the R package 'ggplot'.*

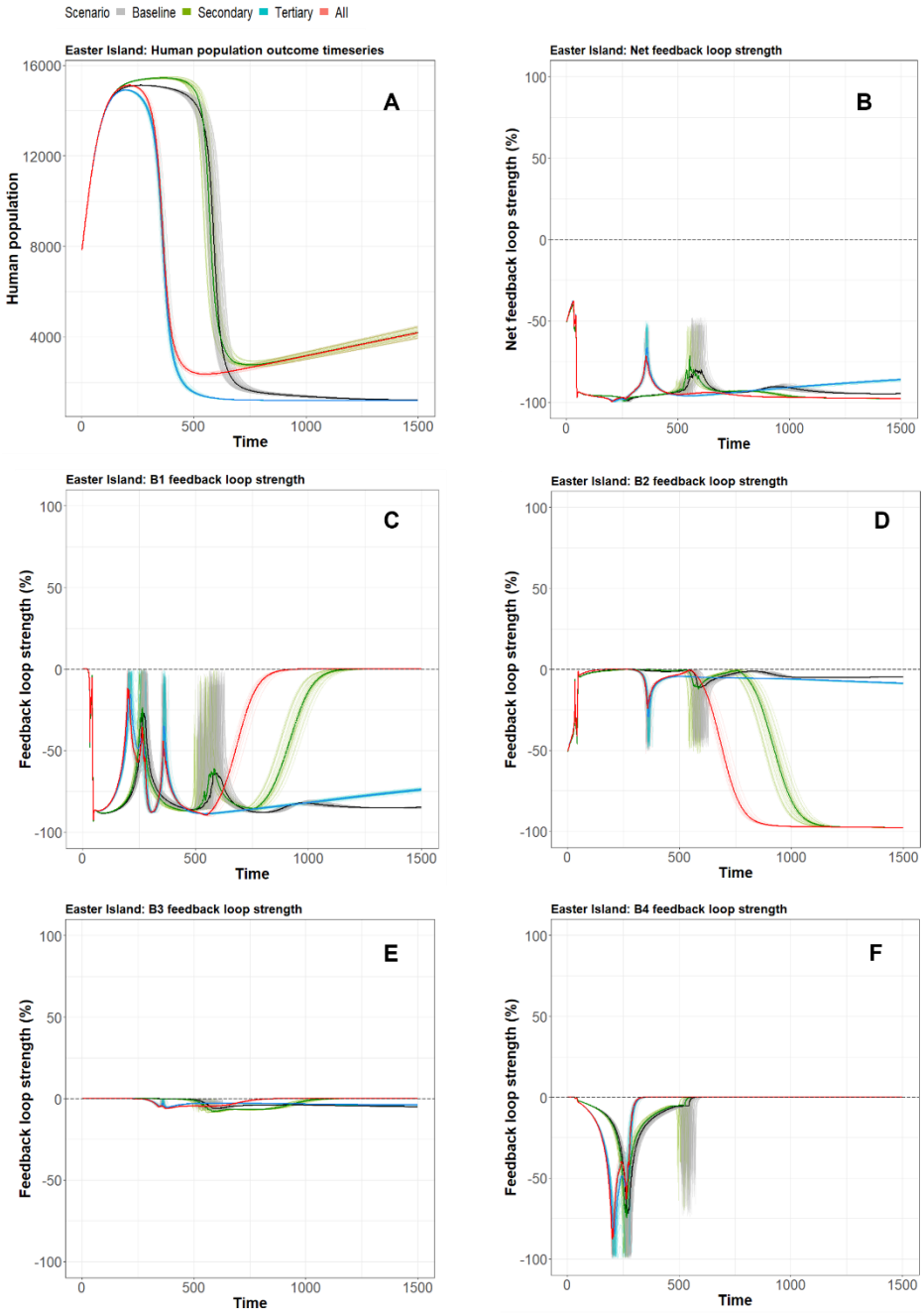

Figure S6-6: Timeseries outcomes from the second LTM experiment (Easter Island) which held the baseline driver trajectory constant but added secondary and tertiary trajectories. *See Table S6-1 for descriptions of the four balancing feedbacks (subplot C-F) responsible for driving the dynamics of the human population (subplot A) over time. Subplots: (A) Timeseries of the modelled Easter Island human population; (B) Timeseries of the net feedback loop strength (i.e., reinforcing minus balancing strengths); (C) Timeseries of percentage contribution of feedback B1 to model behaviour; (D) Timeseries of percentage contribution of feedback B2 to model behaviour; (E) Timeseries of percentage contribution of feedback B3 to model behaviour; (F) Timeseries of percentage contribution of feedback B4 to model behaviour. As per Figure S6-1, simulations within ±0.5% of the median primary driver trajectory are given a transparency value of 1 (i.e., opaque), while all other simulations are given a transparency (alpha value) of 0.05 in the R package 'ggplot'.*

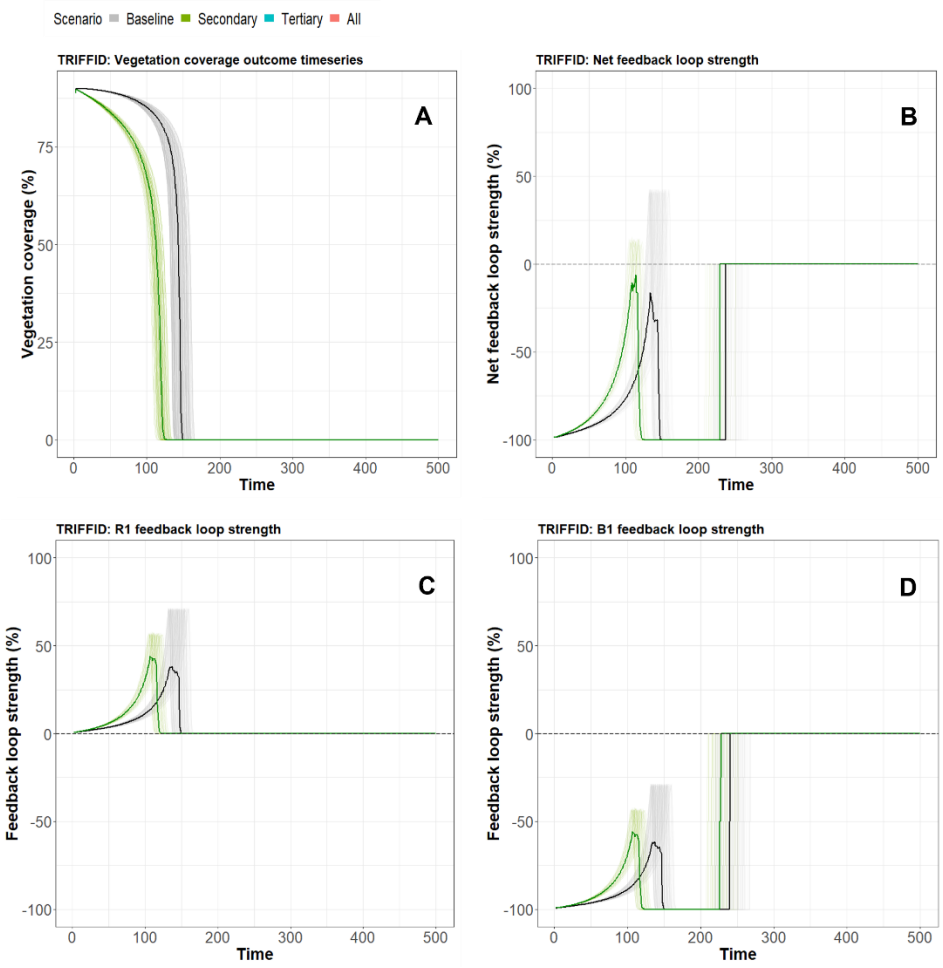

Figure S6-7: Timeseries outcomes from the second LTM experiment (TRIFFID) which held the baseline driver trajectory constant but added secondary and tertiary trajectories. *See Table S6-1 for descriptions of the one reinforcing and one balancing feedback (subplot C-D) responsible for driving the dynamics of the vegetation coverage (subplot A) over time. Subplots: (A) Timeseries of the modelled vegetation coverage; (B) Timeseries of the net feedback loop strength (i.e., reinforcing minus balancing strengths); (C) Timeseries of percentage contribution of feedback R1 to model behaviour; (D) Timeseries of percentage contribution of feedback B1 to model behaviour. As per Figure S6-1, simulations within ±0.5% of the median primary driver trajectory are given a transparency value of 1 (i.e., opaque), while all other simulations are given a transparency (alpha value) of 0.05 in the R package 'ggplot'.*

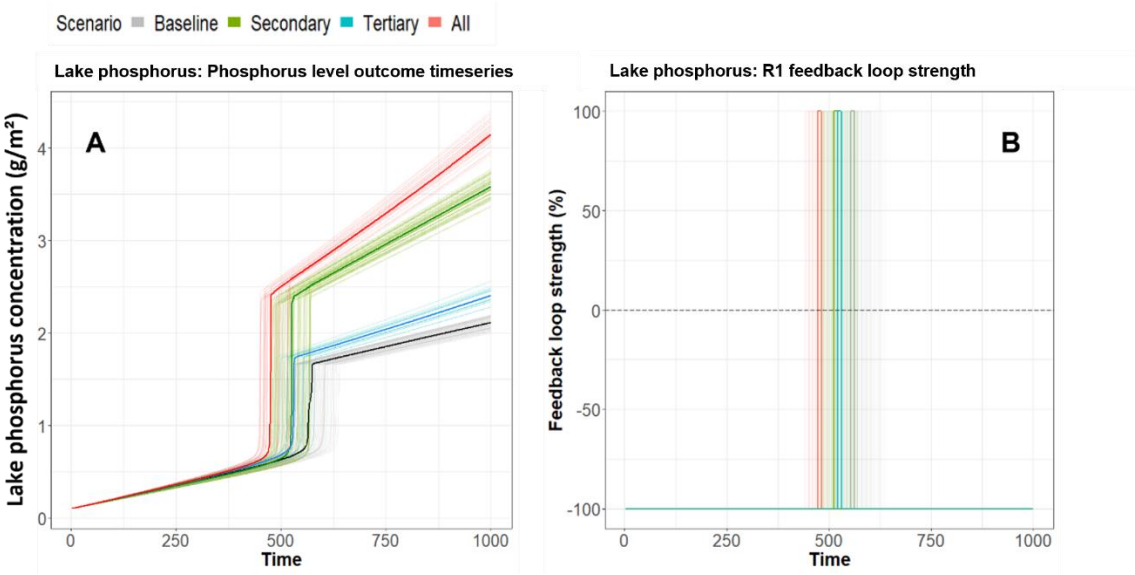

Figure S6-8: Timeseries outcomes from the second LTM experiment (Lake phosphorus) which held the baseline driver trajectory constant (but added secondary and tertiary trajectories. *See Table S6-1 for descriptions of the one reinforcing and one balancing feedback (subplot C-D) responsible for driving the dynamics of the vegetation coverage (subplot A) over time. Subplots: (A) Timeseries of the modelled lake phosphorus levels; (B) Timeseries of the percentage contribution of the single feedback loop to the model behaviour. As per Figure S6-1, simulations within ±0.5% of the median primary driver trajectory are given a transparency value of 1 (i.e., opaque), while all other simulations are given a transparency (alpha value) of 0.05 in the R package 'ggplot'.*

Implications

The feedback loop dynamics depicted in Figures S6-1 to S6-8 help explain the mechanisms driving the breakpoint date timings observed in Figures 2 to 4 (main manuscript). Across each of the four models, Loops That Matter (LTM) analysis indicates that changes in the critical feedbacks driving system stability may be induced earlier either by (a) ramping up the trajectory of the primary stress (Figures S6-1 to S6-4), or (b) adding secondary and tertiary drivers to the system on top of the primary/baseline (Figures S6-5 to S6-8).

These patterns are clearest in the Lake phosphorus model, with only one feedback loop driving the outcomes dynamics. Ramping up the trajectory of phosphorus input into the lake produces earlier spikes in the feedback polarity and strength (e.g., timestep ~870 for the 0.25-0.35 scenario, Figure S6-4), with the gradual increase in lake water phosphorus concentration and phosphorus recycling over time eventually producing a sudden switch to a eutrophic water state. The equivalent pattern also exists for the multi-driver experiment, with the sharp switch to a reinforcing feedback occurring earliest under the 'All' scenario (i.e., timestep 450, Figure S6-8D).

The feedback dynamics of the TRIFFID model are consistent with the Lake phosphorus model, in both the baseline and multi-driver experiments (Figures S6-3 and S6-7, respectively). The increase in the primary driver (temperature) gradually excites the reinforcing feedback over time (Table S6-1), with faster changes in primary driver trajectory leading to earlier onsets in net reinforcing feedback conditions (Figure S6-3C). The abrupt collapse in vegetation coverage (Figure S6-3A) corresponds to this switch from net balancing to net reinforcing feedback conditions, as the loss in vegetation contributes to warmer temperatures, which further contribute to vegetation loss.

Similar to the TRIFFID and Lake phosphorus models, the timing of the collapse in the human population in the Easter Island model corresponds to the net feedback strength becoming less negative (i.e., more positive; Figures S6-2 and S6-6). However, with only four balancing feedbacks in the model (Table S6-1), the individual feedback dynamics in the Easter Island model are different from the TRIFFID and Lake phosphorus models. As the human population grows towards the carrying capacity (Figure S6-2A), we see a strengthening in the balancing feedback which limits tree growth in response to clearance (Figure S6-2G). In turn, instability in the strengths of the balancing feedbacks rises (Figure S6-2D-G) once the land has been cleared beyond a threshold point, with the ecological feedbacks (e.g., rat growth and tree growth) having to reorganise with the eventual loss of the human population. The same pattern emerges under the multi-driver runs in the second LTM experiment, with earlier instability in the 'All' and 'Tertiary' scenarios associated with earlier collapses in the human population (Figure S6-6).

Of the four ecosystem models, the Lake Chilika model has the most complex feedback structure and dynamics[18,21]. During the period of relative fish population stability (approximately 2002-2030, Figure S6-1A), the model is dominated by the two reinforcing feedbacks (Table S6-1) which drive the growth in the traditional and motorised fisher populations over time (Figure S6-1B). As the fisher populations increase, producing higher aggregated fishing efforts (i.e., from more fishing boats), the balancing feedback limiting the effectiveness of motorised fishing efforts (B2, Table S6-1) starts to strengthen in response (Figure S6-1F). In contrast, the balancing feedback limiting traditional fishing efforts remains relatively stable (B1, Table S6-1), owing to (a) only ~20% of fishing boats being traditional from 2020 onwards, and (b) the inferior catch capacities and mobilities of traditional boats. Eventually, the fishing efforts associated with the elevated fisher populations reach unsustainable levels, triggering a collapse in the fish population (which happens earlier under higher rates of human population growth [i.e., the primary driver in the Lake Chilika model]). The subsequent collapse in the fish population limits the number of fisher livelihoods that can be supported by the fishery, and the feedback strengths of the reinforcing feedbacks (R1 and R2) both fall to 0% as the fisher populations shrink in response.

This analysis has attempted to shed light on the feedback loop dynamics behind the ATDC dynamics within the four ecosystem models. For the relatively small and simple TRIFFID and Lake phosphorus models, the ATDC dynamics can be clearly attributed to the growth in a single positive feedback (Table S6-1). This growth tends to occur earlier under scenarios with steeper trajectories of the primary driver, and when the primary driver is combined with additional secondary and tertiary trajectories. However, we tend to see messier feedback trajectories and dynamics in the larger and more complex Easter Island and Lake Chilika models, owing in part to the interconnections between feedback loops which grow and respond to each other. For example, at Lake Chilika, the balancing feedback of declining effectiveness of motorboats, as the fish population declines, is partly coupled to the reinforcing feedback of fisher population growth rate that drives the growth in the motorised fishing population but the collapse in the fish population.

SI7: Supplementary References

1. Barnosky, A. D. *et al.* Approaching a state shift in Earth's biosphere. *Nat. 2012 4867401* **486**, 52–58 (2012).
2. Hughes, T. P., Carpenter, S., Rockström, J., Scheffer, M. & Walker, B. Multiscale regime shifts and planetary boundaries. *Trends Ecol. Evol.* **28**, 389–395 (2013).
3. Biggs, R., Peterson, G. D. & Rocha, J. C. The Regime Shifts Database: a framework for analyzing regime shifts in social-ecological systems. *Ecol. Soc. Publ. online Jul 19, 2018 | doi10.5751/ES-10264-230309* **23**, (2018).
4. Dearing, J. A. *et al.* Safe and just operating spaces for regional social-ecological systems. *Glob. Environ. Chang.* **28**, 227–238 (2014).
5. Lenton, T. M. *et al.* Tipping elements in the Earth's climate system. *Proc. Natl. Acad. Sci. U. S. A.* **105**, 1786–93 (2008).
6. Rocha, J. C., Peterson, G., Bodin, Ö. & Levin, S. Cascading regime shifts within and across scales. *Science (80-.).* **362**, 1379–1383 (2018).
7. Klose, A. K., Karle, V., Winkelmann, R. & Donges, J. F. Emergence of cascading dynamics in interacting tipping elements of ecology and climate. *R. Soc. Open Sci.* **7**, 200599 (2020).
8. Lade, S. J. *et al.* Human impacts on planetary boundaries amplified by Earth system interactions. *Nat. Sustain. 2019 32* **3**, 119–128 (2019).
9. Zeileis, A., Leisch, F., Hornik, K. & Kleiber, C. Package "strucchange". https://cran.r-project.org/web/packages/strucchange/strucchange.pdf (2015).
10. Worm, B. *et al.* Rebuilding Global Fisheries. *Science (80-.).* **325**, 578–585 (2009).
11. Pinsky, M. L., Jensen, O. P., Ricard, D. & Palumbi, S. R. Unexpected patterns of fisheries collapse in the world's oceans. *Proc. Natl. Acad. Sci. U. S. A.* **108**, 8317–8322 (2011).
12. Carpenter, S. R. Eutrophication of aquatic ecosystems: Bistability and soil phosphorus. *Proc. Natl. Acad. Sci. U. S. A.* **102**, 10002–10005 (2005).
13. Matthews, H. D., Gillett, N. P., Stott, P. A. & Zickfeld, K. The proportionality of global warming to cumulative carbon emissions. *Nat. 2009 4597248* **459**, 829–832 (2009).
14. Siteur, K., Eppinga, M. B., Doelman, A., Siero, E. & Rietkerk, M. Ecosystems off track: rate-induced critical transitions in ecological models. *Oikos* **125**, 1689–1699 (2016).
15. Ashwin, P., Wieczorek, S., Vitolo, R. & Cox, P. Tipping points in open systems: bifurcation, noise-induced and rate-dependent examples in the climate system. *Philos. Trans. R. Soc. A Math. Phys. Eng. Sci.* **370**, 1166–1184 (2012).
16. O'Keeffe, P. E. & Wieczorek, S. Tipping Phenomena and Points of No Return in Ecosystems: Beyond Classical Bifurcations. *SIAM J. Appl. Dyn. Syst.* **19**, 2371–2402 (2019).
17. Filatova, T., Polhill, J. G. & van Ewijk, S. Regime shifts in coupled socio-environmental systems: Review of modelling challenges and approaches. *Environ. Model. Softw.* **75**, 333–347 (2016).
18. Cooper, G. S. & Dearing, J. A. Modelling future safe and just operating spaces in regional social-ecological systems. *Sci. Total Environ.* **651**, 2105–2117 (2019).
19. ISEE Systems. STELLA Architect: Systems Thinking for Education and Research. (2018).
20. Schoenberg, W., Davidsen, P. & Eberlein, R. Understanding model behavior using the Loops that Matter method. *Syst. Dyn. Rev.* **36**, 158–190 (2020).
21. Cooper, G. S., Willcock, S. & Dearing, J. A. Regime shifts occur disproportionately faster in larger ecosystems. *Nat. Commun.* **11**, (2020).
22. Brandt, G. & Merico, A. The slow demise of Easter Island: Insights from a modeling investigation. *Front. Ecol. Evol.* **3**, 13 (2015).
23. Cox, P. M. *et al.* Amazonian forest dieback under climate-carbon cycle projections for the 21st century. *Theor. Appl. Climatol. 2004 781* **78**, 137–156 (2004).
24. Ritchie, P. D. L., Clarke, J. J., Cox, P. M. & Huntingford, C. Overshooting tipping point thresholds in a changing climate. *Nat. 2021 5927855* **592**, 517–523 (2021).
25. Carpenter, S. R., Ludwig, D. & Brock, W. A. Management of eutrophication for lakes subject to

potentially irreversible change. *Ecol. Appl.* **9**, 751–771 (1999).
26. Wang, R. *et al.* Flickering gives early warning signals of a critical transition to a eutrophic lake state. *Nature* **492**, 419–422 (2012).